



**HAL**  
open science

## Photoswitchable positive allosteric modulators of metabotropic glutamate receptor 4 to improve selectivity

Silvia Panarello, Aleix González-Díez, Alice E Berizzi, Fanny Malhaire, Roser Borràs-Tudurí, Xavier Rovira, Carme Serra, Laurent Prézeau, Jean-Philippe Pin, Cyril Goudet, et al.

### ► To cite this version:

Silvia Panarello, Aleix González-Díez, Alice E Berizzi, Fanny Malhaire, Roser Borràs-Tudurí, et al.. Photoswitchable positive allosteric modulators of metabotropic glutamate receptor 4 to improve selectivity. *iScience*, 2024, 27 (6), pp.110123. 10.1016/j.isci.2024.110123 . hal-04609139

**HAL Id: hal-04609139**

**<https://hal.science/hal-04609139>**

Submitted on 12 Jun 2024

**HAL** is a multi-disciplinary open access archive for the deposit and dissemination of scientific research documents, whether they are published or not. The documents may come from teaching and research institutions in France or abroad, or from public or private research centers.

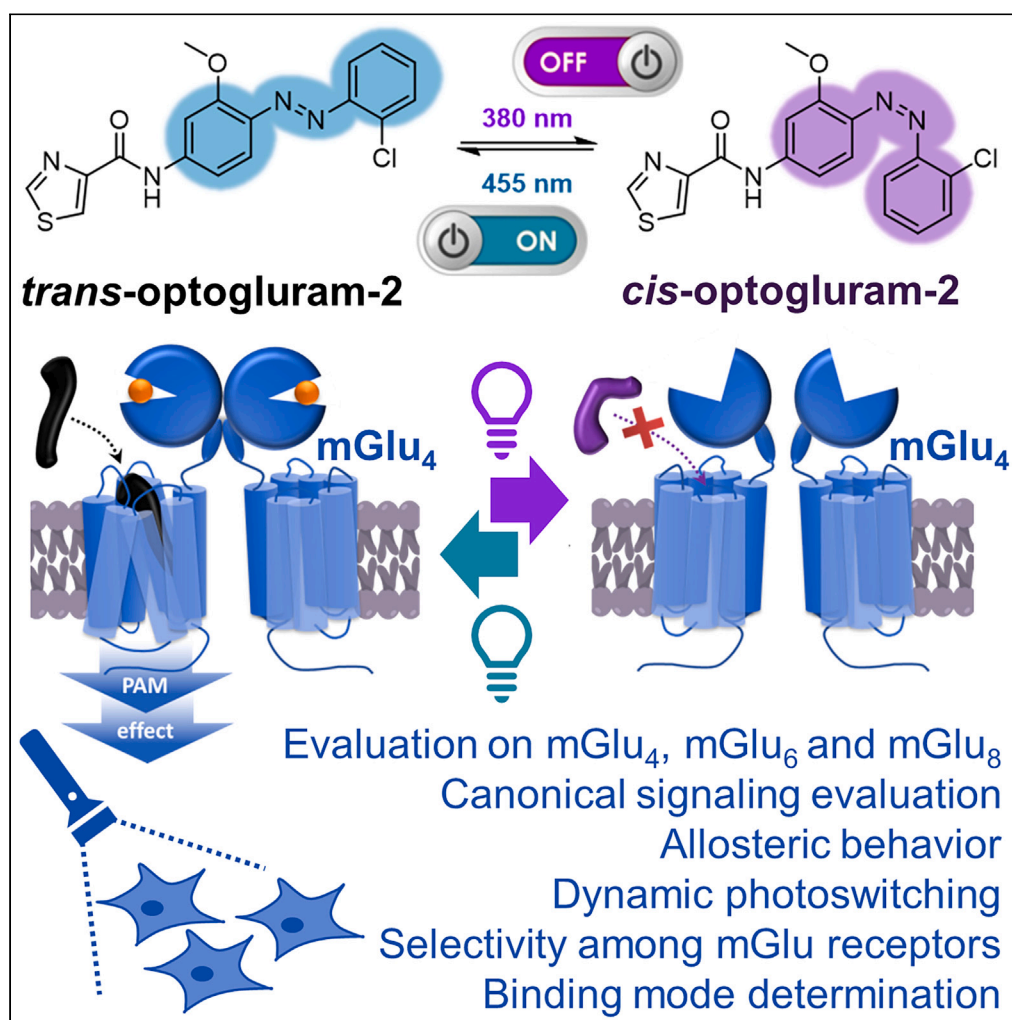
L'archive ouverte pluridisciplinaire **HAL**, est destinée au dépôt et à la diffusion de documents scientifiques de niveau recherche, publiés ou non, émanant des établissements d'enseignement et de recherche français ou étrangers, des laboratoires publics ou privés.



Distributed under a Creative Commons Attribution - NonCommercial 4.0 International License

## Article

## Photoswitchable positive allosteric modulators of metabotropic glutamate receptor 4 to improve selectivity



Silvia Panarello, Aleix González-Díez, Alice E. Berizzi, ..., Cyril Goudet, Amadeu Llebaria, Xavier Gómez-Santacana

amadeu.llebaria@iqac.csic.es (A.L.)  
 xavier.gomez@iqac.csic.es (X.G.-S.)

**Highlights**

A family of optogluram analogs was developed as photoswitchable mGlu<sub>4</sub> PAMs

Optogluram-2 showed an improved selectivity for mGlu<sub>4</sub> over mGlu<sub>6</sub> and mGlu<sub>8</sub> receptors

Optogluram-2 allows switching mGlu<sub>4</sub> activity with 380-nm and 460-nm light wavelengths

Optogluram and optogluram-2 had activity on mGlu<sub>4</sub> as both PAM and allosteric agonists

## Article

## Photoswitchable positive allosteric modulators of metabotropic glutamate receptor 4 to improve selectivity

Silvia Panarello,<sup>1,2,4</sup> Aleix González-Díez,<sup>1,2,5</sup> Alice E. Berizzi,<sup>3,5</sup> Fanny Malhaire,<sup>3</sup> Roser Borràs-Tudurí,<sup>1</sup> Xavier Rovira,<sup>1</sup> Carme Serra,<sup>1</sup> Laurent Prézeau,<sup>3</sup> Jean-Philippe Pin,<sup>3</sup> Cyril Goudet,<sup>3</sup> Amadeu Llebaria,<sup>1,\*</sup> and Xavier Gómez-Santacana<sup>1,3,6,\*</sup>

## SUMMARY

**Metabotropic glutamate receptors (mGlu) regulate multiple functions in the nervous systems and are involved in several neurological disorders. However, selectively targeting individual mGlu subtypes with spatiotemporal precision is still an unmet need. Photopharmacology can address this concern through the utilization of photoswitchable compounds such as optogluram, which is a positive allosteric modulator (PAM) of mGlu<sub>4</sub> that enables the precise control of physiological responses using light but does not have an optimal selectivity profile. Optogluram analogs were developed to obtain photoswitchable PAMs of mGlu<sub>4</sub> receptor with an improved selectivity. Among them, optogluram-2 emerged as a photoswitchable ligand for mGlu<sub>4</sub> receptor with activity as both PAM and allosteric agonists. It presents a higher selectivity and offers improved photoswitching of mGlu<sub>4</sub> activity. These improved properties make optogluram-2 an excellent candidate to study the role of mGlu<sub>4</sub> with a high spatiotemporal precision in systems where mGlu<sub>4</sub> can be co-expressed with other mGlu receptors.**

## INTRODUCTION

G protein-coupled receptors (GPCRs) constitute the largest superfamily of cell surface signaling proteins and regulate many physiological processes through binding a wide variety of endogenous ligands.<sup>1,2</sup> Currently, GPCRs are the target of approximately 35% of drugs and are involved in multiple diseases including infections, inflammation, neurological diseases, cardiovascular diseases, cancer, and endocrine disorders.<sup>3</sup>

The metabotropic glutamate (mGlu) receptors are a family of class C GPCRs comprising eight receptor subtypes subdivided into three different groups based on their sequence homologies, signaling properties, and pharmacology: group I, including mGlu<sub>1</sub> and mGlu<sub>5</sub>; group II, including mGlu<sub>2</sub> and mGlu<sub>3</sub>; and group III, including mGlu receptor subtype 4 (mGlu<sub>4</sub>), mGlu<sub>6</sub>, mGlu<sub>7</sub>, and mGlu<sub>8</sub>.<sup>4</sup> mGlu receptors are widely distributed throughout the central and peripheral nervous system and are endogenously activated by glutamate, the main excitatory neurotransmitter in the vertebrates. Each mGlu subtype has specific roles that can be modulated with orthosteric agonists or antagonists, which compete for the glutamate binding site in the extracellular domain (orthosteric site). There are also allosteric modulators, which act in an alternative binding site usually located in the transmembrane domain (TMD) (allosteric site). The binding of molecules to the allosteric site can result in increased, decreased, or unchanged receptor responses. This leads to positive, negative, or silent allosteric modulators (PAM, NAM, or SAM). Allosteric ligands are generally considered better drug candidates than the orthosteric ligands since they can modulate the receptor activity without interfering with the endogenous ligand binding.<sup>5–7</sup> Additionally, glutamate is the endogenous ligand for a variety of receptor families that are widely distributed in tissues and associated to different physiological effects. Therefore, it is challenging to obtain fully selective ligands targeting glutamate-binding sites. In general, allosteric binding pockets are less well conserved than orthosteric sites and so may allow for the development of selective ligands for specific mGlu subtypes.<sup>8</sup>

The importance of glutamatergic signaling and the modulatory nature of mGlu receptor make them promising drug targets for a variety of psychiatric and neurodegenerative CNS disorders. Therefore, knowledge regarding mGlu receptors has improved exponentially over the last years.<sup>9</sup> In general, targeting glutamatergic neurotransmission via allosteric fine-tuning of mGlu receptor activities holds great promise for the

<sup>1</sup>MCS, Institute for Advanced Chemistry of Catalonia – CSIC, Barcelona, Spain

<sup>2</sup>PhD Program in Organic Chemistry of the University of Barcelona, Barcelona, Spain

<sup>3</sup>Institut de Génomique Fonctionnelle, Université de Montpellier, UMR 5203 CNRS and U 1191 INSERM, Montpellier, France

<sup>4</sup>Present address: Enantia, Barcelona, Spain

<sup>5</sup>These authors contributed equally

<sup>6</sup>Lead contact

\*Correspondence: amadeu.llebaria@iqac.csic.es (A.L.), xavier.gomez@iqac.csic.es (X.G.-S.)

<https://doi.org/10.1016/j.isci.2024.110123>



management of several CNS diseases, with the potential for fewer side effects and a physiological adjustment to glutamate natural release. mGlu<sub>5</sub> and mGlu<sub>2</sub> are the main targets for drug development, but mGlu<sub>4</sub>, mGlu<sub>1</sub>, and mGlu<sub>3</sub> are also promising targets.<sup>10,11</sup>

In particular, there is a growing interest in targeting the mGlu<sub>4</sub> as a therapeutic target to treat diseases, such as Parkinson's disease (PD), epilepsy, anxiety, pain, and fear processing.<sup>12–15</sup> Selective activation of this receptor, via either subtype selective agonists or PAMs, has been shown to significantly reduce or eliminate motor symptoms in preclinical models of PD.<sup>16</sup> Moreover, mGlu<sub>4</sub> PAMs have been proposed as potential novel therapeutics for the palliative treatment of some forms of epilepsy.<sup>17,18</sup> However, the most promising group III allosteric modulators have failed in pre-clinical or clinical phases as possible drug candidates due to adverse effects, lack of efficacy, or cross-activity between the different mGlu subtypes.<sup>19</sup> These issues may be related to the high degree of structural and sequence homology of the allosteric binding pockets, which makes it very difficult to obtain selective modulators<sup>20</sup> but also to the widespread expression of mGlu receptors in different areas of the CNS, which also have different roles depending on the cells in which they are expressed. In this last case, drugs acting in a confined location and time would be desirable.

Indeed, photopharmacology may offer a solution, since it uses the spatiotemporal precision of light to switch on and off the biological activity of target proteins. Photopharmacology makes use of photoswitchable ligands, which are usually derived from existing drugs but include a photoswitch in their molecular scaffold. Thus, the pharmacological properties can be altered upon irradiation with light of different wavelengths (i.e., photoswitching).<sup>21,22</sup> This strategy has been widely applied for research purposes, and several photochromic ligands have been described in the literature allowing the optical control of a wide variety of GPCRs.<sup>23,24</sup> Currently, the use of light-regulated ligands has enabled site-, organ-, tissue-, or even subcellular-specific targeting of mGlu receptors in strictly defined time applications.<sup>25–32</sup>

Regarding group III mGlu receptors, only one photoswitchable PAM has been reported to date. Optogluram (1, Figure 1A) was originally designed by applying an azologization approach<sup>33</sup> on the mGlu<sub>4</sub> PAM VU0415374 (2) (Figure 1B),<sup>34</sup> in which each amide group flanked by aryl groups was replaced by an N=N bridge (i.e., azo bond). This azologization approach gave two different photoswitchable compounds: alloswitch-1, a potent and selective mGlu<sub>5</sub> NAM,<sup>25</sup> and optogluram (1), which was the first photoswitchable ligand for the mGlu<sub>4</sub> receptor.<sup>27</sup> Its azobenzene scaffold allows a rapid isomerization from *trans* to *cis*-configuration upon illumination with violet light (380 nm), and the *trans*-isomer could be quickly recovered from the *cis*-isomer upon green light illumination (500 nm) or by thermal relaxation. *Trans*-optogluram (i.e., in the dark) showed nanomolar mGlu<sub>4</sub> PAM potency, while upon 380-nm illumination its potency was decreased (Figures 1A and 1C).<sup>27</sup> Optogluram (1) was found to be selective over group I and II mGlu receptors, but it was a PAM of mGlu<sub>6</sub> receptor in the micromolar range and, to a lesser extent, of mGlu<sub>8</sub> receptors, both belonging to group III mGlu receptors, as mGlu<sub>4</sub> receptor does.<sup>27</sup>

Since mGlu<sub>6</sub> receptor subtype is differentially expressed to mGlu<sub>4</sub>, optogluram (1) was still considered a good candidate for *in vivo* testing in murine model of inflammatory or neuropathic pain. The application of optogluram (1) in the amygdala of living mice produced acute and reversible analgesic peripheral responses, as well as anxiolytic and antidepressive effects in mice suffering from persistent inflammatory pain. In contrast, those effects were significantly reduced upon 380-nm illumination of the amygdala and subsequently restored with 500 nm light.<sup>27</sup> This allowed a dynamic *on/off* control of pain transmission associated with mGlu<sub>4</sub> receptors localized in the amygdala.<sup>27,35</sup>

Several photoswitchable allosteric modulators for mGlu receptors have been developed but there is still considerable work to complete the photopharmacological toolbox.<sup>36</sup> Besides, obtaining photoswitchable allosteric modulators selectivity among the other mGlu subtypes is highly desirable but it can be challenging in some cases, such as among the group III mGlu receptor subtypes. In this context, we decided to modify the structure of optogluram (1) to generate a small library of azobenzene candidates with the aim of enhancing PAM activity for the mGlu<sub>4</sub> receptor over the other group III mGlu receptors. Additionally, we deciphered the pharmacological characteristics of these azo compounds, including a computational analysis on the binding mode of these allosteric modulators.

## RESULTS

### Design of photoisomerizable azocompounds

The new photoswitchable compounds are based on optogluram (1), the first photoswitchable PAM targeting mGlu<sub>4</sub> receptor.<sup>25,27</sup> During the optimization process, we decided to retain several moieties that are important for related families of previously reported mGlu<sub>4</sub> PAMs (e.g., VU0415374 (2), Figure 1B).<sup>34,37</sup> This includes the outer 2-chlorophenyl ring and the 3-methoxy substituent in the central aromatic ring and the heteroaryl carboxamide. Since many substitutions at the 2-chlorophenyl ring led to a significant decrease in mGlu<sub>4</sub> activity, we decided to focus our efforts on the substitution pattern of the picolinamide moiety and the central phenyl ring of optogluram (1). We also replaced the 2-picolyl group by two different five-membered heteroaryl rings, which is present in other analogs of VU0415374 (2) reported as mGlu<sub>4</sub> PAM.<sup>34,37,38</sup> These modifications provided analogs 3a-d and 4a-b (Figure 1D). Overall, structural modifications to optogluram were designed to enhance mGlu<sub>4</sub> PAM activity over activities at mGlu<sub>6/8</sub> receptors.

### Synthesis of optogluram analogs 3a-d and 4a-b

Optogluram analogs 3a-d and 4a-b were prepared following an optimized two-step synthetic route (Scheme 1), in contrast to the 5-step original route used to synthesize optogluram (1). The sequence started with the direct diazotization of 2-chloroaniline (5) followed by the azo-coupling with 3-methoxyaniline (6a) or 2-chloro-5-methoxyaniline (6b) to yield amino azobenzenes 7a and 7b. These amines were acylated with the corresponding carboxylic acids 8a-b, 9, and 10 to give azo compounds 3a-d and 4a-b.

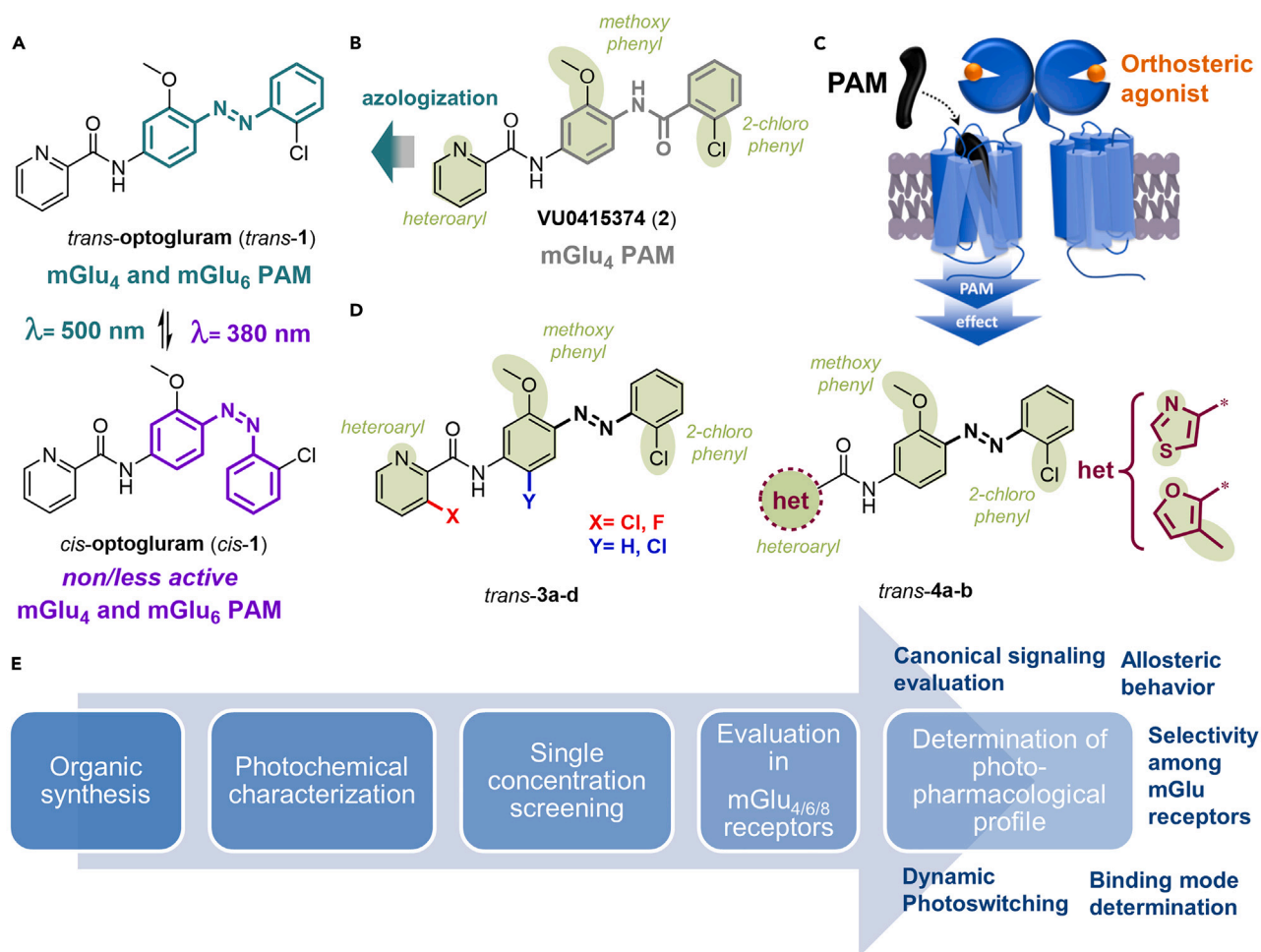


**Figure 1. Design of photoisomerizable azocompounds as photoswitchable positive allosteric modulators for mGlu<sub>4</sub> receptor**

(A) Structure of optogluram (1) as the first photoswitchable allosteric ligand for mGlu<sub>4</sub> receptor. Optogluram photoisomerizes from *trans* to *cis* configuration or vice versa upon illumination with different wavelengths.

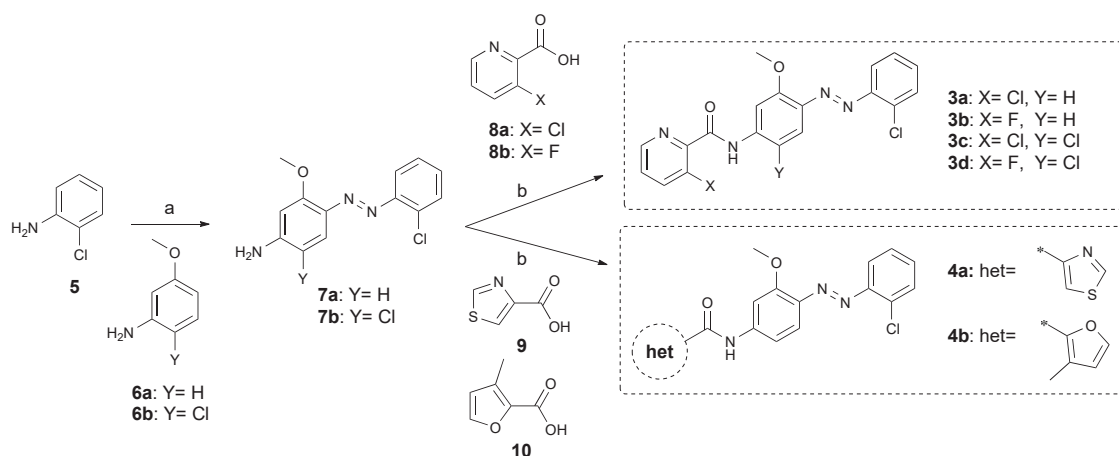
(B) Optogluram resulted from an azologization strategy applied to VU0415374 (2), a reported mGlu<sub>4</sub> PAM (C). Both *trans*-optogluram and VU0415374 positive allosteric modulators (PAMs, in black) bind in the allosteric pocket of mGlu<sub>4</sub> receptor at the mGlu<sub>4</sub> transmembrane domain, in contrast to orthosteric agonists (in orange) that bind in the extracellular domains.

(D) Optimization plan for mGlu<sub>4</sub> PAM optogluram (1) to maintain the activity in mGlu<sub>4</sub> conserving moieties highlighted in green and decrease potency at mGlu<sub>6/8</sub> receptors via analogs 3a-d and 4a-b. (E) Flow diagram illustrating the steps followed in the present manuscript.

### Photochemical characterization

The photochemical properties of 3a-d and 4a-b were investigated by UV/vis absorption spectroscopy using different illumination conditions. As expected from azo compounds, samples in the dark presented the archetypical profile of *trans* *p*-N-amido azobenzenes including the typical *trans*-azobenzene  $\pi$ - $\pi^*$  transition band at 380–390 nm (Figures 2A, 2B, and S1).<sup>27,39</sup> Upon illumination with different wavelengths between 365 and 560 nm, we detected a mixture of different proportions of the *cis* and the *trans* isomers in the photostationary state (PSS), which depended on the illumination wavelength. As expected, *cis* isomers showed a  $\pi$ - $\pi^*$  transition band at 270–300 nm and a weaker  $n$ - $\pi^*$  transition band near 430 nm, which is forbidden by the symmetry for *trans* azobenzenes. The highest proportions of *cis* isomers for all the six azo compounds were obtained upon 380-nm illumination and were back-isomerized to their thermodynamically stable *trans* isomer by either using turquoise light (455–470 nm) (Figures 2A, 2B, and S1) or allowing them to thermally isomerize in the dark (Figure S2). The reversibility of the photoisomerization was determined by following the absorbance change upon applying several 380/455-nm alternate illumination cycles. No considerable differences were observed, showing robust photoisomerization with no apparent degradation (Figure 2C).

The photoisomerization of azo compound 4a in DMSO was examined by liquid chromatography-tandem mass spectrometry and compared to optogluram (1). In the dark, 98.6%  $\pm$  0.1% of *trans*-4a was observed, whereas a PSS of 73.0%  $\pm$  0.5% *cis*-4a was detected after 385-nm illumination. Subsequent illumination with 470 nm wavelength afforded a PSS of 56.1%  $\pm$  1.2% *trans*-4a (Figures 2 and S3). As expected, due to the similar structural characteristics of the azobenzene moiety, these values were in line with those obtained for



### Scheme 1. Synthesis of optogluram analogs 3a-d and 4a-b

Reagents and conditions: (A) (I) conc. HCl, NaNO<sub>2</sub>, 0°C, 20 min; (II) NaOAc, 0°C, 30 min, 57%–85%; (B) HATU, TEA, DMF, 40°C–60°C, 16–48 h, 21%–79%.

optogluram: 100% of *trans* isomer in the dark, 75.7% ± 0.4% *cis*-1 upon 385-nm illumination, and 57.2% ± 0.2% after exposure to 470-nm light (Figure S3). We additionally explored the thermal *cis*-to-*trans* isomerization of compound **4a** in aqueous solution with different proportions of DMSO and compared it to that of optogluram (**1**). In general, the *cis*-isomer half-lives were shorter for compound **4a**, and both compounds showed faster relaxation when the proportion of DMSO was lower, only remaining for few minutes in aqueous solutions with 5% DMSO (Figure S2).

### Pharmacological characterization of 3a-d and 4a-b with IP accumulation assays

As optogluram (**1**) mainly showed PAM activity in mGlu<sub>4</sub> and mGlu<sub>6</sub> receptors in previous studies,<sup>27</sup> the putative activity of azo compounds **3a-d** and **4a-b** was determined using a cell-based inositol phosphate (IP) accumulation assay with HEK293 cells transiently expressing either the mGlu<sub>4</sub> or mGlu<sub>6</sub> receptor and a chimeric G<sub>αq/i</sub> protein, which enables the functional coupling of these receptors to the IP pathway. We first

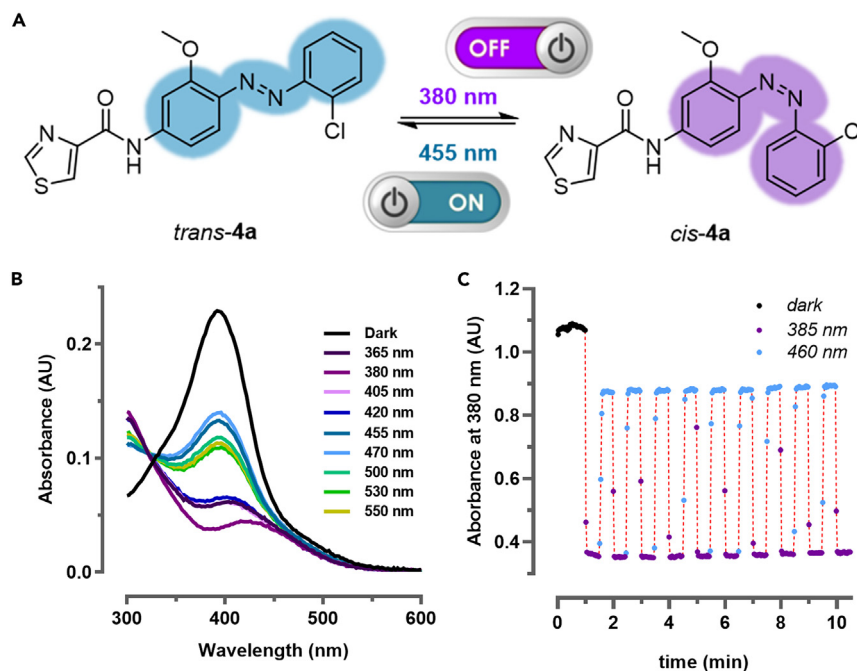


**Figure 2. Photochemical characterization of compound 4a**

(A) Scheme of *trans/cis* isomerization of compound **4a**; (B) UV/vis absorption spectra of **4a** 25 μM in DMSO at 25°C under dark (black) and different light conditions for 3 min; (C) UV/vis absorption measurements every 2 s of 100 μM **4a** in DMSO at λ<sub>π-π\*</sub>max of *trans* isomer (380 nm) under continuous illumination with 385 (violet) or 460 nm light (turquoise).

screened the compounds at a single concentration (30  $\mu\text{M}$ ) at the mGlu<sub>4</sub> and mGlu<sub>6</sub> with a constant concentration of an orthosteric agonist (i.e., L-AP<sub>4</sub>, 5 nM or 100 nM for mGlu<sub>4</sub> and for mGlu<sub>6</sub> receptors, respectively) to explore the putative PAM activity. These measurements were done in parallel in the dark and under 380 nm illumination conditions. Compounds **3c** and **3d** had reduced activity compared to the control PAM VU0415374 (**2**) in both mGlu<sub>4</sub> and mGlu<sub>6</sub> receptors (Figure S4). Based on these data, we confirmed that the addition of a substituent in the 6-position of the central ring would drastically reduce the activity at both mGlu<sub>4</sub> and mGlu<sub>6</sub> receptors. In contrast, the remaining compounds at 30  $\mu\text{M}$  activated mGlu<sub>4</sub> and, to a reduced extent, the mGlu<sub>6</sub> receptor (Figure S4), a welcomed departure for the next experiments.

The functional activity of **3a-b** and **4a-b** was further studied through concentration-response curves in an IP accumulation assay in HEK293 cells expressing either the human isoform of mGlu<sub>4</sub>, mGlu<sub>6</sub>, or mGlu<sub>8</sub> receptors. To evaluate the light-dependent effects, we used the same increasing concentrations of the compounds in the dark and under illumination at 380 nm in parallel. As a result, we generated concentration-response curves that allowed us to obtain the potencies (EC<sub>50</sub>) for each compound under both conditions (Table 1; Figures S5 and S6). Considering the activity on mGlu<sub>4</sub> receptor, we observed that the four compounds displayed an activity in the low micromolar range in the dark, but only azo compounds **3b** and **4a** had potencies in line with optogluram (**1**), whereas compounds **3a** and **4b** displayed potencies significantly lower (Tables S1 and S3). Of note, the potencies of optogluram (**1**) in mGlu<sub>8</sub> and mGlu<sub>6</sub> human isoforms resulted very similar. This is contrasting with the previous reported results of optogluram (**1**) using the rat isoforms, which had lower potency at the mGlu<sub>8</sub> isoform as compared to the using mGlu<sub>6</sub> isoform.<sup>27</sup> Within the present series, only compound **3a** showed no significant activity in mGlu<sub>6</sub> receptor, and compound **4a** appeared to be the least active of the series at mGlu<sub>8</sub> receptor. Compounds **3b** and **4b** displayed a potency similar to optogluram (**1**) at mGlu<sub>8</sub> receptor (Figure S6). When considering the assays performed under illumination, we noted that 380-nm irradiation induced a right shift of the dose-response curves as expected. This effect was compatible with a loss of the PAM potency of the *cis* isomers. This confirms that the active isomers of these new azobenzene candidates are the *trans* isomers, supporting the *trans*-on optogluram-like approach (Table 1; Figure S5). Unexpectedly, the observed photoinduced potency shift seems larger in the four azo compounds **3a-b** and **4a-b** than in optogluram (**1**), which might induce an improved *on/off* photoswitching in more complex assays (Table 1; Figure S5).

Overall, compounds **3b** and **4a** displayed an activity similar to optogluram (**1**) but only compound **4a** displays a satisfactory selectivity over mGlu<sub>6</sub> and mGlu<sub>8</sub> receptors, since compound **3b** still had considerable PAM activity on mGlu<sub>6</sub> and mGlu<sub>8</sub> receptors (Figure S6). Besides, compound **4a** has a slightly higher photoinduced potency shift (PPS) after illuminating at 380 nm (PPS = 0.55 log-fold) compared to that of optogluram (**1**, PPS = 0.46 log-fold). All these results indicate that compound **4a** emerged as the mGlu<sub>4</sub> photoswitchable PAM with the best profile to date.

### Pharmacological characterization of **4a** cAMP accumulation assays

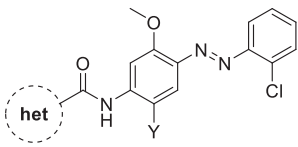
We decided to further characterize the pharmacological properties of compound **4a**, named optogluram-2. First, we wanted to confirm the results obtained in mGlu<sub>4</sub> receptor using the G<sub>αi/o</sub> canonical pathway for the mGlu<sub>4</sub> receptor, since the IP accumulation assays involve the activation of the G<sub>αq</sub> pathway, requiring a chimeric G protein. Thus, we generated concentration-response curves of **4a**, together with optogluram (**1**) and compounds **3a-b** and **4b** using a cyclic adenosine monophosphate (cAMP) accumulation assay and an inducible stable HEK293 cell line expressing the rat isoform of mGlu<sub>4</sub> receptor. As performed before, the light-dependent effects were evaluated in parallel, simultaneously generating two curves for each of the four azo-PAMs active, in the dark and under illumination at 380 nm. Unexpectedly, all compounds showed significantly improved potency with EC<sub>50</sub> values in the nanomolar range ( $8.4 \leq \text{pEC}_{50} \leq 6.6$ , Tables S1 and S4; Figures 3A and S7). This was in contrast to the results obtained with the IP accumulation assays, which were in the low micromolar range. Compounds **3b** and **4a** had a similar potency in the dark in the cAMP accumulation assay, as compared to **3a** and **4b**, which were significantly less active (Table S3). Compound **4a** was the most potent of the four azo compounds and the one that showed the greatest photoinduced potency shift (PPS = 1.3 log-fold) after illumination at 380 nm, being larger than that for optogluram (PPS = 1.0 log-fold, Table S1; Figures 3A and S7).

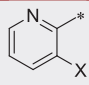
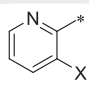
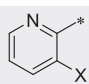
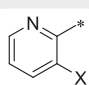
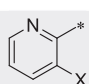
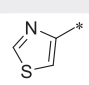
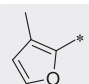
To explore the reasons for the difference in potency ranges between IP and cAMP accumulation assays, and considering that we were comparing human and rat mGlu<sub>4</sub> isoforms, we also performed the IP accumulation assays with HEK293 cells transiently expressing rat mGlu<sub>4</sub> receptor (Table S1; Figure S8). The resulting potencies for compounds **3a-b** and **4a-b** were slightly higher than those resulting from human isoform, but still in the micromolar range ( $\Delta\text{pEC}_{50} = 0.2\text{--}0.4$ ) and not significantly different (Table S4). Therefore, the difference in potency between IP and cAMP accumulation assays cannot be associated to the human or rat isoform of mGlu<sub>4</sub> receptor, but to the intrinsic characteristics of each assay. As the aforementioned differences in activity are not observed for the orthosteric agonist L-AP<sub>4</sub>, our hypothesis is that the mGlu<sub>4</sub>-G complex may be slightly different depending on the associated G protein (G<sub>αq/i</sub> vs. G<sub>i</sub>). As a result, the PAMs, such as optogluram analogs or VU0415374, may exhibit a higher affinity for the mGlu<sub>4</sub>-G<sub>i</sub> complex.

### Allosteric interaction of optogluram or optogluram-2 with L-AP<sub>4</sub>

We next studied the pharmacological profile of optogluram-2 (**4a**) in comparison with optogluram (**1**) by means of concentration-response curves of the agonist L-AP<sub>4</sub> in the presence of different concentrations of the allosteric modulators using the same cAMP accumulation assay. The measurements were performed both in dark and under illumination conditions at 380 nm (Figures 3B and S9). The obtained data were plotted as the percentage of decrease of cAMP to account for the increase of mGlu<sub>4</sub> activity prompted by the agonist and fitted with an operational model of allostery (Equation 2). As expected, the results confirm a similar positive cooperativity (i.e., increase in agonist potency) in the dark for both photoswitchable PAMs as the agonist curve is shifted to the left with increasing concentrations of the PAM. Besides, both azobenzene PAMs also induced an increase of basal activity, which is commonly associated with allosteric agonism (i.e., ago-PAM) (Figure 3C), also comparable for both compounds. However, this might also be a result of potentiation of the agonistic effect of the residual endogenous

**Table 1. Photoisomerization and pharmacological properties of analogs 3a-d and 4a-b**



Cpd.	het	X	Y	Photoisomerization		Pharmacological characterization					
				$\lambda_{\max} (\pi-\pi^*)^a$ [nm]		hmGlu <sub>4</sub> <sup>d</sup>		hmGlu <sub>6</sub> <sup>d</sup>		hmGlu <sub>8</sub> <sup>d</sup>	
				<i>trans</i> <sup>b</sup>	<i>PSS</i> <sub>380</sub> <sup>c</sup>	pEC <sub>50</sub> ± SEM	<i>PSS</i> <sub>380</sub> <sup>c</sup>	<i>trans</i> <sup>b</sup>	<i>PSS</i> <sub>380</sub> <sup>c</sup>	<i>trans</i> <sup>b</sup>	<i>PSS</i> <sub>380</sub> <sup>c</sup>
Optogluram (1)		H	H	ND	ND	6.0 ± 0.1	5.5 ± 0.2	5.3 ± 0.0	<5.0	5.3 ± 0.1	<5.0
3a		Cl	H	385	434	5.2 ± 0.1	<4.5	<4.5	n.a.	<5.0	n.a.
3b		F	H	391	434	5.7 ± 0.1	<5.0	<5.0	<4.5	<5.0	n.a.
3c		Cl	Cl	391	436	<4.5	<4.5	ND	ND	ND	ND
3d		F	Cl	390	432	<4.5	<4.5	ND	ND	ND	ND
4a		-	H	385	433	5.7 ± 0.1	5.2 ± 0.1	<4.5	n.a.	<4.5	n.a.
4b		-	H	390	435	5.3 ± 0.1	<4.5	<4.5	n.a.	<5.0	n.a.
L-AP <sub>4</sub>	-	-	-	-	-	6.9 ± 0.1	7.2 ± 0.2	5.9 ± 0.1	6.0 ± 0.1	7.0 ± 0.2	6.9 ± 0.5

<sup>a</sup>The absorbance maxima for compounds were extracted from UV/vis spectra (25 μM in DMSO at 25°C).

<sup>b</sup>Experiments were performed in the dark to characterize 100% *trans* isomer.

<sup>c</sup>Photostationary state upon illumination with 380 nm light to obtain a high percentage of *cis* isomer.

<sup>d</sup>The pharmacological experiments were performed with an IP accumulation assays using HEK293 cells transiently expressing the corresponding mGlu receptor subtype. Values are means ± SEM of minimum 3 independent values. Values < 5.0 correspond to pEC<sub>50</sub> between 4.5 and 5.0, obtained with partial function fitting. Values < 4.5 may include replicates with non-convergent fitting. n.a., not showing activity in a minimum of 2 independent replicates. ND, non-determined.

glutamate that the cells naturally produce, even though, this is unlikely as the original compound, VU0415374 (2), has been reported to be an ago-PAM with a very similar allosteric profile.<sup>40</sup> As expected for *trans*-on photoswitchable ligands, both PAM effects were considerably lower upon 380-nm illumination (Figure S9).

### Assessment of the reversibility of mGlu<sub>4</sub> photoswitching

We next evaluated the reversibility of the mGlu<sub>4</sub>-activity photoswitching induced by optogluram and optogluram-2 to confirm that the different pharmacological effect of *cis* and *trans* isomers can be dynamically switched with light. Thus, we used HEK293 cells expressing both mGlu<sub>4</sub> receptor and a fluorescence resonance energy transfer (FRET)-based cAMP biosensor.<sup>41</sup> First, mGlu<sub>4</sub> activity was measured after 60 min of cell incubation with L-AP<sub>4</sub> and the photoswitchable PAMs in the dark. Then, the cells were continuously illuminated with 380-nm light for 10 min to read once again the FRET and, immediately after, the cells were illuminated with 470 nm light for 10 additional minutes to finally determine the recovery of mGlu<sub>4</sub> activity. As expected, after the period in the dark, illumination with 380-nm light induced an increase of cytosolic cAMP. This was compatible with a decrease of the activity of mGlu<sub>4</sub> receptor induced by the photoisomerization of the two compounds



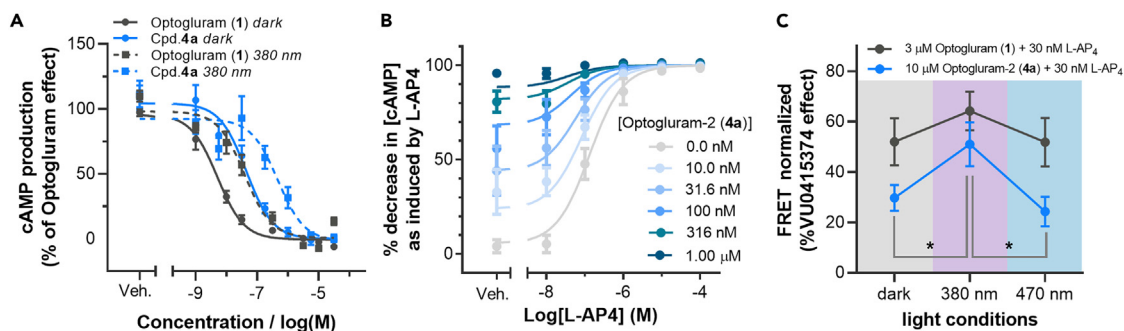


**Figure 3. Pharmacological characterization of optogluram-2 (4a)**

(A) Concentration-response curve of optogluram-2 (4a) with a constant concentration of L-AP<sub>4</sub> 5 nM in HEK293 stable rat mGlu<sub>4</sub> cell line with a cAMP assay in dark conditions (rounded spots and blue solid line) and under illumination at 380 nm of wavelength (square dots and blue dotted line). Optogluram (1) was used as a photoswitchable mGlu<sub>4</sub> PAM standard in dark conditions (round dots and gray solid line) and under illumination at 380 nm (square dots and gray dotted line). Values are means of 4 independent values with SEM as error bars.

(B) Effect of different concentrations of optogluram-2 (4a) on L-AP<sub>4</sub> concentration-dependent activation of mGlu<sub>4</sub> receptor as determined by cAMP measurement, in dark conditions. Optogluram-2 (4a) modulates positively the agonistic effect of L-AP<sub>4</sub> and elicits intrinsic agonist activity in its *trans* configuration. Values are means of minimum 6 independent values with SEM as error bars.

(C) Receptor function could be dynamically controlled in a reversible manner by optogluram-2 (4a) using a cytosolic cAMP biosensor and upon the application of consecutive illuminations of 380 and 470 nm light. Values are means of 4 independent values with SEM as error bars. Two-way ANOVA with time as repeated measure and including the Dunnett correction for multiple testing, \* $p < 0.05$ . Non-significant for optogluram (1).

to the less active *cis* isomer. The change in the biological response after the illumination was found to be larger for optogluram-2 (4a), in agreement with IP and cAMP accumulation experiments (Figure 3C). This effect was reversed by turquoise illumination demonstrating a reversible photoswitching in the cellular assays as well as a dynamic control of the biological activity of the mGlu<sub>4</sub> receptor with light (Figure 3C).

### Selectivity profile among the mGlu subtypes

The selectivity profile of optogluram-2 (4a) was also explored for the remaining human mGlu subtypes at a single concentration of 30 μM with different concentrations of agonists, which was depending on the mGlu subtype and the desired effect to measure: PAM or NAM activity (Figures 4 and S10). Additionally, the selectivity of compound 4a was compared with the selectivity of optogluram (1). We used the IP accumulation assay in HEK293 cell overexpressing the corresponding receptors. Despite being slightly less potent than optogluram (1) as mGlu<sub>4</sub> PAM, optogluram-2 (4a) was found to activate mGlu<sub>4</sub> receptor at 30 μM concentration with a significant selectivity over the other seven mGlu subtypes. In contrast, optogluram (1) was also active as PAM of mGlu<sub>6</sub> and mGlu<sub>8</sub> receptors, showing no significant difference of activity in such assay (Figures 4 and S10). The activity observed for compound 1 and 4a at the rest of mGlu subtypes (mGlu<sub>1-3,5,7</sub>) was not significant, except for optogluram (1) in mGlu<sub>3</sub> ( $p = 0.0174$ , *t* test, Table S6).

### Computational studies

To gain wider insight on the different pharmacological properties of optogluram (1) and optogluram-2 (4a) and understand the molecular basis of optogluram-2 mGlu<sub>4/6/8</sub> selectivity, we examined the molecular ligand interactions on the allosteric pocket of mGlu<sub>4</sub>, mGlu<sub>6</sub>, and mGlu<sub>8</sub> receptors using computational tools (Figures 5 and S11). In our model of mGlu<sub>4</sub> based on the reported cryoelectron microscopy (cryo-EM) structure of this receptor (PDB code 7E9H), VU0415374 (2, Figure S11A) was positioned in a hydrophobic allosteric binding pocket inside the TM7 bundle, similar to other allosteric sites previously described for mGlu receptors. VU0415374 (2) was positioned in a transversal manner allowing a strong interaction with W798<sup>6,50</sup> via hydrogen bond and  $\pi$ - $\pi$  stacking. Additionally, the ligand establishes a hydrogen bond with S825<sup>7,36</sup> (Figure S11A). Despite observing a similar pose for *trans*-optogluram (1) and *trans*-optogluram-2 (4a), this latter interaction was not feasible since these molecules lack the amide bond (Figures 5A and 5D). Instead, optogluram (1) and optogluram-2 (4a) interact through a hydrogen bond with a serine residue in TM7 (S827<sup>7,40</sup> and S825<sup>7,40</sup>, in mGlu<sub>6</sub> and mGlu<sub>8</sub>, respectively) probably promoting these ligands to increase the distance with the top of TM6. This difference may explain the higher potency of VU0415374 compared to its azologs 1 and 4b. In contrast, the models with the three ligands showed very similar hydrophobic interactions and the strong interaction with W798<sup>6,50</sup>. Indeed, W798<sup>6,50</sup> is known by mutagenesis to be crucial for class C GPCR function and is also believed to adopt different rotameric states depending on the active/inactive conformation of the receptor.<sup>40,42-44</sup> For instance, the rotameric state of the W798<sup>6,50</sup> in mGlu<sub>4</sub> and the closely related mGlu<sub>6</sub> and mGlu<sub>8</sub> receptors differ in crystal structures of inactive receptors, such as mGlu<sub>1</sub> (PDB: 4OR2) or mGlu<sub>5</sub> (PDB: 6FFI, 7P2L).<sup>45-47</sup> The docking of optogluram (1) and optogluram-2 (4b) in *cis* configuration did not retrieve results to be analyzed, further reinforcing the idea that only the *trans* isomers have the ability to bind these receptors.

We next examined the binding mode of VU0415374 (2), optogluram (1), and optogluram-2 (4a) using models of the mGlu<sub>6</sub> and mGlu<sub>8</sub> transmembrane domain based on the cryo-EM structure of mGlu<sub>4</sub> receptor (PDB: 7E9H, Figures 5B, 5C, 5E, 5F, S11B, and S11C).<sup>48</sup> Docking

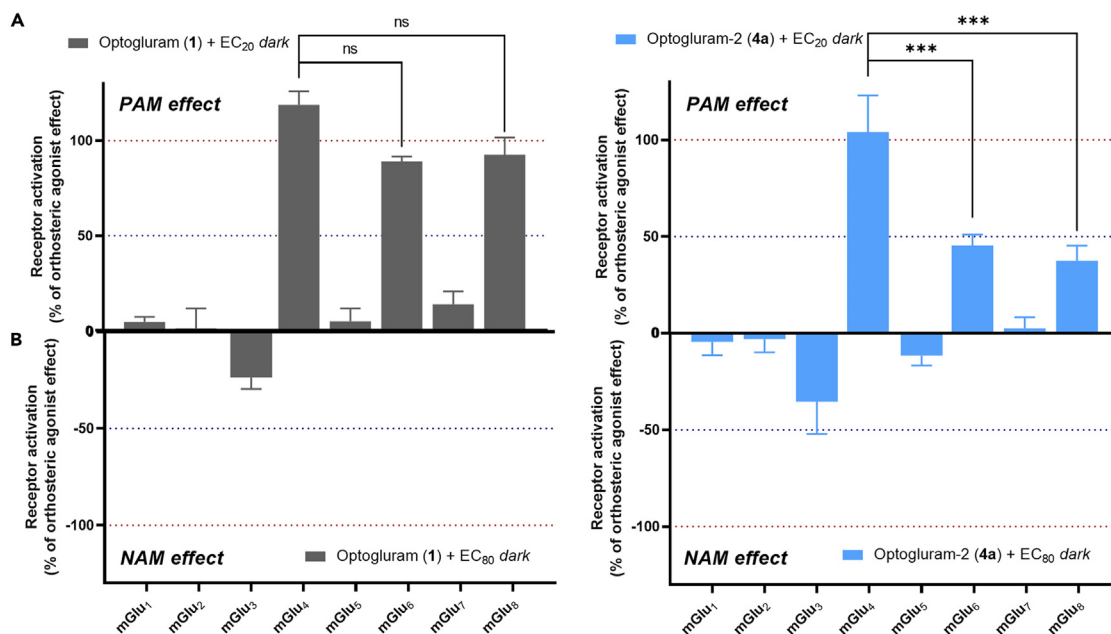


**Figure 4. Selectivity profile of optogluram (1) and optogluram-2 (4a) among the mGlu subtypes**

(A and B) Compounds 1 and 4a were tested at 30  $\mu$ M among the eight human mGlu subtypes as PAM (A) and as NAM (B) in dark conditions. For the PAM effect evaluation, 0% corresponds to activation induced by the low dose of orthosteric agonist and 100% to the activation induced by saturating concentrations of orthosteric agonist. For the NAM effect evaluation, 0% corresponds to the activation induced by a high dose of orthosteric agonist and -100% to the basal activity with no agonist. Values are means of minimum 3 replicates with SEM as error bars. Two-way ANOVA including the Dunnett correction for multiple testing between mGlu<sub>4</sub> effect with the other mGlu subtypes, showing significant differences with  $p < 0.0001$ , with the exception of the comparisons indicated in the graph between mGlu<sub>4</sub> and mGlu<sub>6/8</sub>, which are significant for optogluram-2, but not for optogluram (\*\* $p < 0.001$ , ns  $p > 0.05$ ).

studies of optogluram and optogluram-2 (Figures 5B, 5C, 5E, and 5F) showed a similar binding mode as VU0415574 (Figure S11C). Although the binding pocket between mGlu<sub>4</sub>, mGlu<sub>6</sub>, and mGlu<sub>8</sub> receptors is highly conserved, the binding mode of the three PAMs adopted a more vertical pose compared to the binding mode observed in mGlu<sub>4</sub>. The presence of T661<sup>3,40</sup> in the allosteric pocket of mGlu<sub>6</sub> receptor (in contrast to M663<sup>3,40</sup> in mGlu<sub>4</sub> receptor), the interaction of the amide with S827<sup>7,40</sup> in mGlu<sub>6</sub> and S825<sup>7,40</sup> in mGlu<sub>8</sub>, and extra hydrogen bond of the pyridine ring with S825<sup>7,40</sup> in the case of mGlu<sub>8</sub> could lock the ligand in a more vertical position preventing the hydrogen bond with W796<sup>6,50</sup> as observed for mGlu<sub>4</sub> receptor. The resulting weaker interaction of the three compounds with W796<sup>6,50</sup> in the mGlu<sub>6</sub> and mGlu<sub>8</sub> models may explain the decreased PAM potency with regard to mGlu<sub>4</sub>. On the other hand, the residue in positions 7.40 and 3.40 are described to enhance the receptor activation in mGlu<sub>5</sub> receptor (S809<sup>7,40</sup> and P665<sup>3,40</sup>, respectively) and, therefore, they may play a similar role in mGlu<sub>6</sub> and mGlu<sub>8</sub> receptors.<sup>43,49,50</sup> The pyridine (VU0415374 and optogluram)/thiazole ring (optogluram-2) was positioned adjacent to Y665<sup>3,44</sup> and Y663<sup>3,44</sup> in mGlu<sub>6</sub> and mGlu<sub>8</sub>, presumably interacting by means of  $\pi$ - $\pi$  stacking. This interaction might explain the difference in potency between the two compounds, as a  $\pi$ - $\pi$  stacking with the thiazole ring would be expected weaker than with pyridine.<sup>51,52</sup>

## DISCUSSION

Photopharmacology is an emerging discipline already consolidated in the field of GPCRs and currently provides novel tool compounds to help the scientific community unravel the complexity of GPCRs signaling and organization.<sup>24</sup> In contrast to conventional drugs, photopharmacology makes use of light-sensitive ligands, which include small-molecule photoswitchable ligands<sup>25,53–55</sup> but also tethered photoswitchable ligands,<sup>56,57</sup> photoswitchable peptides,<sup>58</sup> and caged ligands.<sup>59</sup> Such photopharmacological strategies have been applied to several GPCRs, including histamine,<sup>53</sup> dopamine,<sup>56</sup> serotonin,<sup>57</sup> adenosine,<sup>55</sup> opioid,<sup>59</sup> chemokine,<sup>54</sup> GLP-1,<sup>58</sup> or mGlu receptors,<sup>25</sup> among others, and offer the possibility to precisely control activity duration at a particular location, providing a next level of selectivity: spatiotemporal selectivity. One of the first examples to have shown such selectivity in a rodent preclinical model was optogluram (1), an azobenzene-based positive allosteric modulator of mGlu<sub>4</sub> receptor. Using this photoswitchable ligand, we demonstrated an on/off photoswitching of mGlu<sub>4</sub> activity that allowed the control of pain sensitivity with light cycles. Thus, we validated the role of mGlu<sub>4</sub> receptor in amygdala as a key signaling effector bypassing central sensitization processes to dynamically modulate chronic pain symptoms.<sup>27,35</sup> However, the mGlu receptor subtype selectivity of optogluram was not optimal, since it was also activating mGlu<sub>6</sub>, and in a lower degree mGlu<sub>8</sub> receptor. Given the restricted expression of mGlu<sub>6</sub> receptor, predominantly in retina,<sup>60</sup> this lack of selectivity does not hinder the study of mGlu<sub>4</sub> biological function in different brain areas. However, the selectivity of optogluram limits its use to explore the roles of mGlu receptors in visual glutamate signaling, as there is evidence that both mGlu<sub>6</sub> and mGlu<sub>4</sub> receptors are expressed in retina.<sup>61–63</sup> In addition, we discovered that the PAM activity of optogluram

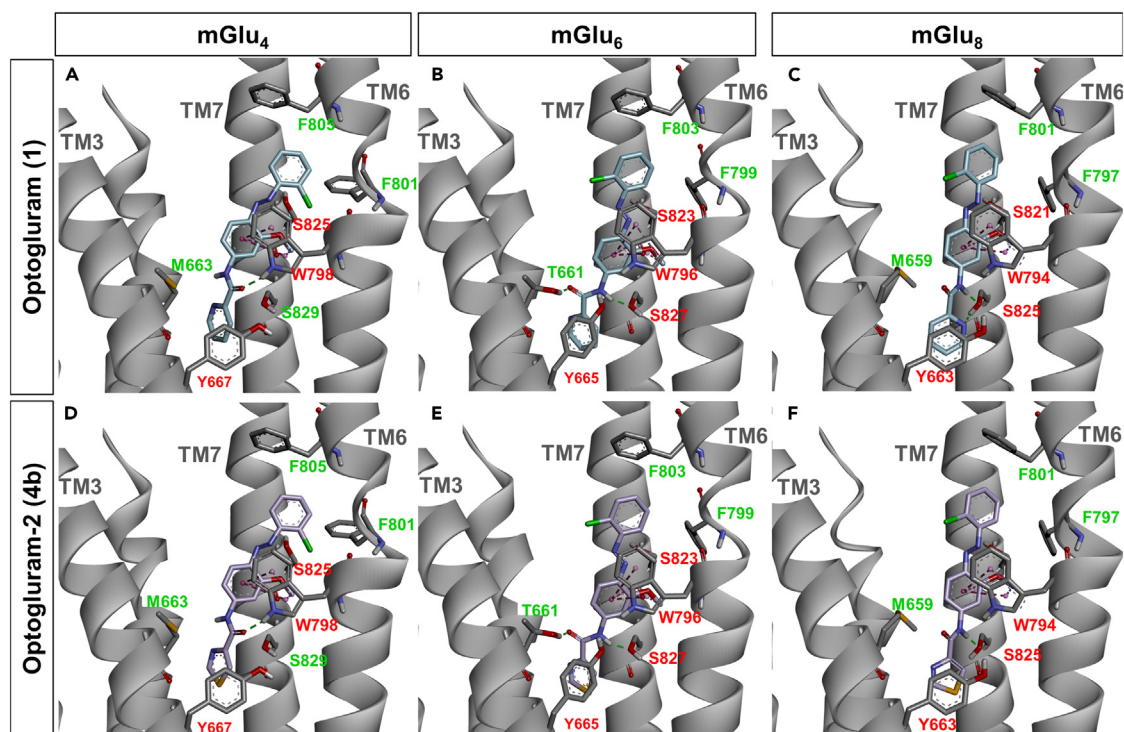


**Figure 5. Computational studies of optogluram and optogluram-2**

Binding mode of optogluram (1, cyan; A, B, and C) and optogluram-2 (4a, violet; D, E, and F) in the allosteric site inside the TM7 bundle of the cryo-EM structure of mGlu<sub>4</sub> receptor<sup>48</sup> (A and D, PDB: 7E9H), the homology model of mGlu<sub>6</sub> receptor (B and E) and the homology model of mGlu<sub>8</sub> receptor (C and F). Key residues are annotated, including those performing the most important interactions in red. Green dashed lines correspond to hydrogen bonds and purple dashed lines to hydrophobic interactions. The models were generated using Glide-XP<sup>65</sup> (Schrödinger, LLC, New York, NY, 2024). TM1 and TM5 are not shown to facilitate visual interpretation.

on the human isoform of mGlu<sub>8</sub> receptor was higher than on the rat variants, reaching a similar activity to that obtained with mGlu<sub>6</sub> receptors. These limitations prompted the search for obtaining a photoswitchable compound selective for mGlu<sub>4</sub> receptors to distinguish from the effects associated with mGlu<sub>8</sub> receptors, located on presynaptic glutamatergic neurons in the brain, or mGlu<sub>6</sub> receptor in retina.

In the present work, we synthesized a small library of photoswitchable analogs of optogluram changing the substitution of the central or pyridine ring with the aim of conserving mGlu<sub>4</sub> activity and expecting to lose mGlu<sub>6</sub> and mGlu<sub>8</sub> activity. These modifications did not induce a major change of the azobenzene nature, obtaining photochromic compounds with a comparable photoisomerization profile. Indeed, the photostationary states between optogluram (1) and optogluram-2 (4b) resulted very similar and both compounds shared a modest *cis*-to-*trans* isomerization under turquoise illumination. However, the rapid thermal relaxation in aqueous media may lead to a high proportion of *trans* isomer in a few minutes, which is sufficient for our purposes. These photoisomerization properties are similar to other photoswitchable allosteric modulators for mGlu receptors, including alloswitch-1<sup>30</sup> and aBINA.<sup>31</sup> Additionally, both alloswitch-1 and optogluram were found to have excellent photoswitching properties in experiments *in vivo*,<sup>26,27,30,35</sup> indicating that a moderate photoisomerization *in vitro* may induce considerable changes in highly regulated physiological systems.

We found that azocompound 4a (optogluram-2) acted as a PAM of mGlu<sub>4</sub> receptor using an IP accumulation assay with a chimeric G<sub>q</sub> protein. In such assay, optogluram-2 had slightly reduced potency than optogluram but had an improved selectivity over other mGlu receptors, promoting a significantly lower activation of the group III mGlu<sub>6</sub> and mGlu<sub>8</sub> receptors, which was not observed with optogluram. The difference in potency between optogluram and optogluram-2 was preserved when their activity was studied at the rat mGlu<sub>4</sub> receptor in an IP accumulation assay and also in a cAMP accumulation assay, which monitors the canonical signaling pathway. In all cases, optogluram-2 had slightly improved photoswitching following 380-nm illumination, as compared to the reference azocompound optogluram. The reversibility of the mGlu<sub>4</sub>-activity photoswitching was confirmed using illumination with violet (380 nm) and turquoise (470 nm) light. In general, the photoswitching observed for optogluram-2 was higher than that observed for optogluram, involving a sensible improvement of photoregulation of mGlu<sub>4</sub> activity. The faster *cis*-to-*trans* relaxation rate of optogluram-2 may also contribute to a more significant mGlu<sub>4</sub> photoswitching after 470 nm illumination. We also studied the type of allosteric modulation of optogluram and optogluram-2 by means of functional interactions with L-AP<sub>4</sub>, and the results suggested that both PAMs potentiated the orthosteric agonist activity to similar extents and have comparable intrinsic activity (i.e., they are ago-PAMs) at equipotent concentrations.

Computational modeling shown here suggests that diamide compound **VU0415374** and azo compounds optogluram and optogluram-2 share a similar binding mode in the allosteric pocket inside the TMD of mGlu<sub>4</sub> receptor. Very recently, during our manuscript writing step, a new different binding mode has been reported in a novel mGlu<sub>4</sub> cryo-EM structure for the structurally related PAM VU0364770. In this structure, the shorter bicyclic VU0364770 is bound in the interprotomeric interface between TM1, 6, 7 and TM6 from each subunit, respectively.<sup>64</sup> In contrast, we proposed a binding site for PAMs **1**, **2**, and **4a** in the active subunit between helices TM2, 3, 6, 7, which is in very good agreement with previous mutagenesis studies in mGlu<sub>4</sub> receptor with the tricyclic **VU0415374** (**2**) and other similar PAMs.<sup>40</sup> We hypothesize that both binding pockets may exist in mGlu<sub>4</sub> homodimer, where either two PAMs may bind or one pocket may be a vestibule for the second one. However, proving this hypothesis would need several experiments and it is out of the scope of the present study. The binding site found for the three compounds in mGlu<sub>6</sub> and mGlu<sub>8</sub> receptor homology models was located in the same region of the TMD. However, the binding mode was slightly different, adopting a more vertical pose in mGlu<sub>6</sub> and mGlu<sub>8</sub> TMDs. For these receptors, the binding mode was characterized for having weaker but more numerous interactions. Among them, it is important to point out hydrophobic interactions between Tyr665<sup>3,44</sup> and the ligand heterocyclic ring. Indeed,  $\pi$ - $\pi$  stacking energies may be very different depending on the nature of the heterocycles<sup>51,52</sup> and that would explain the difference of activity between optogluram and optogluram-2 in mGlu<sub>6</sub> and mGlu<sub>8</sub> receptors.

Overall, on the characterization process of the series of optogluram analogs, compound **4b** (optogluram-2) has emerged as a new photoswitchable PAM of the mGlu<sub>4</sub> receptor with improved photoswitching behavior and selectivity among the other mGlu subtypes. In particular, optogluram-2 can be used as a tool to explore the pathophysiologic function of mGlu<sub>4</sub> *in vitro*, *ex vivo* in brain slices, or *in vivo* in animal models of neuropathic pain or PD. As compared to optogluram (**1**), for which the specificity of the response observed required the use of knockout mice,<sup>27</sup> the optimized selectivity of optogluram-2 (**4a**) toward mGlu<sub>4</sub> may enable to discriminate more precisely the contribution of mGlu<sub>4</sub> versus mGlu<sub>6</sub> or mGlu<sub>8</sub> in the eye or in brain areas where these receptors are expressed concomitantly.<sup>60</sup> In conclusion, optogluram-2 constitutes a novel potential candidate to study the roles of mGlu<sub>4</sub> receptor with improved spatiotemporal precision and shows an advancement in the field for the development of subtype selective mGlu<sub>4</sub> PAMs that may inspire the development of future studies involving allosteric modulators for mGlu receptors.

### Limitations of the study

Although optogluram-2 is a photoswitchable tool compound that has improved certain limitations of its parent analog optogluram, its activity has not been demonstrated in models *in vivo*. This will be explored in future studies. Furthermore, certain properties of the optogluram family of photoswitchable mGlu<sub>4</sub> PAMs could be further improved. This includes the increase of the mGlu<sub>4</sub> PAM potency and improvement of the photoisomerization properties in order to obtain photostationary states richer in one of the azobenzene isomers to enhance photoinduced potency shift.

Optogluram and optogluram-2 are photoswitchable mGlu<sub>4</sub> PAMs in their stable *trans* configuration, and illumination with 380 nm light leads to photoisomerization to less active isomer. Although they are excellent tool compounds, an approach in which *trans* isomers are not active in the dark but can be activated with illumination is more interesting from the therapeutic point of view, in order to obtain high spatiotemporal precision of drug action. Future research on mGlu<sub>4</sub> photopharmacology and, specifically, on photoswitchable allosteric modulators must take into account these questions.

### STAR★METHODS

Detailed methods are provided in the online version of this paper and include the following:

- KEY RESOURCES TABLE
- RESOURCE AVAILABILITY
  - Lead contact
  - Materials availability
  - Data and code availability
- EXPERIMENTAL MODEL AND STUDY PARTICIPANT DETAILS
- METHOD DETAILS
  - Organic synthesis and chemical characterisation
  - Photochemical characterisation
  - Pharmacological characterisation
  - Computational methods
- QUANTIFICATION AND STATISTICAL ANALYSIS

### SUPPLEMENTAL INFORMATION

Supplemental information can be found online at <https://doi.org/10.1016/j.isci.2024.110123>.

## ACKNOWLEDGMENTS

We thank Lourdes Muñoz from SIMChem (IQAC-CSIC) for the use of analytical support and helpful discussions, ARPEGE Pharmacology-Screening-Interactome platform facility (UMS Bio-campus, Montpellier, France) for the use of the plate readers, Revvity (former PerkinElmer-Cisbio) for providing HTRF cAMP and IPOne kits in the frame of EIDOS collaborative laboratory, and H. Gutierrez-de-Teran for computational support. The results included in this standard have received funding from the European Union's Horizon 2020 research and innovation program under Marie Skłodowska-Curie grant agreement no. 801342 (Tecnospring INDUSTRY, TECSPR19-1-0062) and the Government of Catalonia's Agency for Business Competitiveness (ACCIÓ) to X.G.-S., Agence Nationale de la Recherche (ANR-17-CE11-0046) to J.-P.P., Labex EpiGenMed (ANR-10-LABX-12-01) to J.-P.P., Fondation pour la Recherche Médicale (FRM DEQ20170336747) to J.-P.P., from the NEURON Research Program which is jointly funded by national funding authorities within the framework of the ERA-NET Neuron (ANR-17-NEU3-0001) to C.G. and A.L., the CNRS International Scientific Collaboration Program (PICS 08212) to C.G., A.L., and X.R., Ministerio de Ciencia e Innovación, Agencia Estatal de Investigación, and ERDF - A way of making Europe (CTQ2017-89222-R, PCI2018-093047, PID2020-120499RB-I00, and PIE-RYC2020-029485-I) to A.L. and X.R., by the Agència de Gestió d'Ajuts Universitaris i de Recerca (2021 SGR 00508) to A.L. and by the Spanish National Research Council (20228AT014) to X.R. We thank the European Research Network on Signal Transduction (ERNEST Cost Action 18133) and the International Research Network on GPCRs (iGPCRnet) to finance the diffusion of our research.

## AUTHOR CONTRIBUTIONS

Conceptualization, S.P., A.L., and X.G.-S.; methodology, S.P., A.E.B., A.G.-D., F.M., X.R., and X.G.-S.; validation, C.S., L.P., J.-P.P., C.G., X.R., A.L., and X.G.-S.; formal analysis, L.P., X.R., and X.G.-S.; investigation, S.P., A.G.-D., A.E.B., R.B.-T., and X.G.-S.; resources, S.P., A.G.-D., A.E.B., F.M., R.B.-T., and C.S.; writing – original draft, S.P., A.G.-D., A.L., and X.G.-S.; writing – review and editing, A.E.B., J.-P.P., C.G., X.R., A.L., and X.G.-S.; visualization, S.P. and X.G.-S.; supervision, C.S., L.P., J.-P.P., C.G., X.R., A.L., and X.G.-S.; funding acquisition, J.-P.P., C.G., X.R., A.L., and X.G.-S.

## DECLARATION OF INTERESTS

J.-P.P. is the scientific director of Eidos, a common laboratory with the private company Revvity. He is acting as a consultant for Givaudan and Pharvaris.

Received: November 29, 2023

Revised: March 15, 2024

Accepted: May 24, 2024

Published: May 28, 2024

## REFERENCES

1. Fredriksson, R., Lagerström, M.C., Lundin, L.G., and Schiöth, H.B. (2003). The G-protein-coupled receptors in the human genome form five main families. Phylogenetic analysis, paralogon groups, and fingerprints. *Mol. Pharmacol.* 63, 1256–1272. <https://doi.org/10.1124/mol.63.6.1256>.
2. Schiöth, H.B., and Lagerström, M.C. (2008). Structural diversity of G protein-coupled receptors and significance for drug discovery. *Nat. Rev. Drug Discov.* 7, 339–357. <https://doi.org/10.1038/nrd2518>.
3. Sriram, K., and Insel, P.A. (2018). GPCRs as targets for approved drugs: How many targets and how many drugs? *Mol. Pharmacol.* 93, 251–258. <https://doi.org/10.1124/MOL.117.111062>.
4. Gregory, K.J., and Goudet, C. (2021). International Union of Basic and Clinical Pharmacology. CXI. Pharmacology, Signaling, and Physiology of Metabotropic Glutamate Receptors. *Pharmacol. Rev.* 73, 521–569. <https://doi.org/10.1124/PR.119.019133>.
5. Sheffler, D.J., Gregory, K.J., Rook, J.M., and Conn, P.J. (2011). Allosteric Modulation of Metabotropic Glutamate Receptors. In *Advances in Pharmacology* (Elsevier Inc.), pp. 37–77. <https://doi.org/10.1016/B978-0-12-385952-5.00010-5>.
6. Stansley, B.J., and Conn, P.J. (2019). Neuropharmacological Insight from Allosteric Modulation of mGlu Receptors. *Trends Pharmacol. Sci.* 40, 240–252. <https://doi.org/10.1016/j.tips.2019.02.006>.
7. Bian, Y., Jun, J.J., Cuyler, J., and Xie, X.Q. (2020). Covalent allosteric modulation: An emerging strategy for GPCRs drug discovery. *Eur. J. Med. Chem.* 206, 112690. <https://doi.org/10.1016/j.ejmech.2020.112690>.
8. Luessen, D.J., and Conn, P.J. (2022). Allosteric Modulators of Metabotropic Glutamate Receptors as Novel Therapeutics for Neuropsychiatric Disease. *Pharmacol. Rev.* 74, 630–661. <https://doi.org/10.1124/PHARMREV.121.000540>.
9. Witkin, J.M., Pandey, K.P., and Smith, J.L. (2022). Clinical investigations of compounds targeting metabotropic glutamate receptors. *Pharmacol. Biochem. Behav.* 219, 173446. <https://doi.org/10.1016/j.pbb.2022.173446>.
10. Nickols, H.H., and Conn, P.J. (2014). Development of allosteric modulators of GPCRs for treatment of CNS disorders. *Neurobiol. Dis.* 61, 55–71. <https://doi.org/10.1016/j.nbd.2013.09.013>.
11. Nicoletti, F., Bruno, V., Ngomba, R.T., Gradini, R., and Battaglia, G. (2015). Metabotropic glutamate receptors as drug targets: what's new? *Curr. Opin. Pharmacol.* 20, 89–94. <https://doi.org/10.1016/j.coph.2014.12.002>.
12. Calabrese, V., Picconi, B., Heck, N., Campanelli, F., Natale, G., Marino, G., Sciacaluga, M., Ghiglieri, V., Tozzi, A., Anceaume, E., et al. (2022). A positive allosteric modulator of mGlu4 receptors restores striatal plasticity in an animal model of L-Dopa-induced dyskinesia. *Neuropharmacology* 218, 109205. <https://doi.org/10.1016/j.neuropharm.2022.109205>.
13. Raber, J., and Duvoisin, R.M. (2015). Novel metabotropic glutamate receptor 4 and glutamate receptor 8 therapeutics for the treatment of anxiety. *Expert Opin. Investig. Drugs* 24, 519–528. <https://doi.org/10.1517/13543784.2014.986264>.
14. Pereira, V., and Goudet, C. (2019). Emerging trends in pain modulation by metabotropic glutamate receptors. *Front. Mol. Neurosci.* 11, 424363. <https://doi.org/10.3389/fnmol.2018.00464/BIBTEX>.
15. Davis, M.J., Iancu, O.D., Acher, F.C., Stewart, B.M., Eiwaz, M.A., Duvoisin, R.M., and Raber, J. (2013). Role of mGluR4 in acquisition of fear learning and memory. *Neuropharmacology* 66, 365–372. <https://doi.org/10.1016/j.neuropharm.2012.07.038>.
16. Panarese, J.D., Engers, D.W., Wu, Y.J., Bronson, J.J., Macor, J.E., Chun, A.,

- Rodriguez, A.L., Felts, A.S., Engers, J.L., Loch, M.T., et al. (2019). Discovery of VU2957 (Valiglurax): An mGlu 4 Positive Allosteric Modulator Evaluated as a Preclinical Candidate for the Treatment of Parkinson's Disease. *ACS Med. Chem. Lett.* 10, 255–260. <https://doi.org/10.1021/acsmchemlett.8b00426>.
17. Marino, M.J., Hess, J.F., and Liverton, N. (2005). Targeting the Metabotropic Glutamate Receptor mGluR4 for the Treatment of Diseases of the Central Nervous System. *Curr. Top. Med. Chem.* 5, 885–895. <https://doi.org/10.2174/1568026054750263>.
  18. Celli, R., Santolini, I., Van Luijckelaer, G., Ngomba, R.T., Bruno, V., and Nicoletti, F. (2019). Targeting metabotropic glutamate receptors in the treatment of epilepsy: rationale and current status. *Expert Opin. Ther. Targets* 23, 341–351. <https://doi.org/10.1080/14728222.2019.1586885>.
  19. Rascol, O., Medori, R., Baayen, C., Such, P., and Meulien, D.; AMBLED Study Group (2022). A Randomized, Double-Blind, Controlled Phase II Study of Foliglurax in Parkinson's Disease. *Mov. Disord.* 37, 1088–1093. <https://doi.org/10.1002/MDS.28970>.
  20. Lindsley, C.W., Emmitte, K.A., Hopkins, C.R., Bridges, T.M., Gregory, K.J., Niswender, C.M., and Conn, P.J. (2016). Practical Strategies and Concepts in GPCR Allosteric Modulator Discovery: Recent Advances with Metabotropic Glutamate Receptors. *Chem. Rev.* 116, 6707–6741. <https://doi.org/10.1021/acs.chemrev.5b00656>.
  21. Szymański, W., Beierle, J.M., Kistemaker, H.A.V., Velema, W.A., and Feringa, B.L. (2013). Reversible photocontrol of biological systems by the incorporation of molecular photoswitches. *Chem. Rev.* 113, 6114–6178. <https://doi.org/10.1021/cr300179f>.
  22. Hüll, K., Morstein, J., and Trauner, D. (2018). In Vivo Photopharmacology. *Chem. Rev.* 118, 10710–10747. <https://doi.org/10.1021/acs.chemrev.8b00037>.
  23. Ricart-Ortega, M., Font, J., and Llebaria, A. (2019). GPCR Photopharmacology (Elsevier). <https://doi.org/10.1016/j.mce.2019.03.003>.
  24. Panarello, S., Rovira, X., Llebaria, A., and Gómez-Santacana, X. (2022). Photopharmacology of G-Protein-Coupled Receptors. In *Molecular Photoswitches: Synthesis, Properties and Applications*, Z.L. Pianowski, ed. (Wiley-VCH GmbH), pp. 921–944. <https://doi.org/10.1002/9783527827626.CH37>.
  25. Pittolo, S., Gómez-Santacana, X., Eckelt, K., Rovira, X., Dalton, J., Goudet, C., Pin, J.P., Llobet, A., Giraldo, J., Llebaria, A., and Gorostiza, P. (2014). An allosteric modulator to control endogenous G protein-coupled receptors with light. *Nat. Chem. Biol.* 10, 813–815. <https://doi.org/10.1038/nchembio.1612>.
  26. Gómez-Santacana, X., Pittolo, S., Rovira, X., Lopez, M., Zussy, C., Dalton, J.A.R., Faucherre, A., Jopling, C., Pin, J.P., Ciruela, F., et al. (2017). Illuminating Phenylazopyridines to Photoswitch Metabotropic Glutamate Receptors: From the Flask to the Animals. *ACS Cent. Sci.* 3, 81–91. <https://doi.org/10.1021/acscentsci.6b00353>.
  27. Zussy, C., Gómez-Santacana, X., Rovira, X., De Bundel, D., Ferrazzo, S., Bosch, D., Asede, D., Malhaire, F., Acher, F., Giraldo, J., et al. (2018). Dynamic modulation of inflammatory pain-related affective and sensory symptoms by optical control of amygdala metabotropic glutamate receptor 4. *Mol. Psychiatry* 23, 509–520. <https://doi.org/10.1038/mp.2016.223>.
  28. Rovira, X., Trapero, A., Pittolo, S., Zussy, C., Faucherre, A., Jopling, C., Giraldo, J., Pin, J.P., Gorostiza, P., Goudet, C., and Llebaria, A. (2016). OptoGluNAM4.1, a Photoswitchable Allosteric Antagonist for Real-Time Control of mGlu4 Receptor Activity. *Cell Chem. Biol.* 23, 929–934. <https://doi.org/10.1016/j.chembiol.2016.06.013>.
  29. Bossi, S., Helleringer, R., Galante, M., Monlleó, E., Trapero, A., Rovira, X., Daniel, H., Llebaria, A., and McLean, H. (2018). A light-controlled allosteric modulator unveils a role for mGlu4 receptors during early stages of ischemia in the rodent cerebellar cortex. *Front. Cell. Neurosci.* 12, 449. <https://doi.org/10.3389/fncel.2018.00449>.
  30. Ricart-Ortega, M., Berizzi, A.E., Pereira, V., Malhaire, F., Catena, J., Font, J., Gómez-Santacana, X., Muñoz, L., Zussy, C., Serra, C., et al. (2020). Mechanistic Insights into Light-Driven Allosteric Control of GPCR Biological Activity. *ACS Pharmacol. Transl. Sci.* 3, 883–895. <https://doi.org/10.1021/acspstsci.0c00054>.
  31. Donthamsetti, P., Konrad, D.B., Hetzler, B., Fu, Z., Trauner, D., and Isacoff, E.Y. (2021). Selective Photoswitchable Allosteric Agonist of a G Protein-Coupled Receptor. *J. Am. Chem. Soc.* 143, 8951–8956. <https://doi.org/10.1021/jacs.1c02586>.
  32. Pittolo, S., Lee, H., Lladó, A., Tosi, S., Bosch, M., Bardia, L., Gómez-Santacana, X., Llebaria, A., Soriano, E., Colombelli, J., et al. (2019). Reversible silencing of endogenous receptors in intact brain tissue using 2-photon pharmacology. *Proc. Natl. Acad. Sci. USA* 116, 13680–13689. <https://doi.org/10.1073/pnas.1900430116>.
  33. Morstein, J., Awale, M., Reymond, J.L., and Trauner, D. (2019). Mapping the Azolog Space Enables the Optical Control of New Biological Targets. *ACS Cent. Sci.* 5, 607–618. <https://doi.org/10.1021/acscentsci.8b00881>.
  34. Engers, D.W., Field, J.R., Le, U., Zhou, Y., Bolinger, J.D., Zamorano, R., Blobaum, A.L., Jones, C.K., Jadhav, S., Weaver, C.D., et al. (2011). Discovery, synthesis, and structure-activity relationship development of a series of N-(4-acetamido)phenylpicolinamides as positive allosteric modulators of metabotropic glutamate receptor 4 (mGlu(4)) with CNS exposure in rats. *J. Med. Chem.* 54, 1106–1110. <https://doi.org/10.1021/jm101271s>.
  35. Pereira, V., Arias, J.A., Llebaria, A., and Goudet, C. (2023). Photopharmacological manipulation of amygdala metabotropic glutamate receptor mGlu4 alleviates neuropathic pain. *Pharmacol. Res.* 187, 106602. <https://doi.org/10.1016/j.phrs.2022.106602>.
  36. Gómez-Santacana, X., Panarello, S., Rovira, X., and Llebaria, A. (2022). Photoswitchable allosteric modulators for metabotropic glutamate receptors. *Curr. Opin. Pharmacol.* 66, 102266. <https://doi.org/10.1016/j.coph.2022.102266>.
  37. Jones, C.K., Engers, D.W., Thompson, A.D., Field, J.R., Blobaum, A.L., Lindsley, S.R., Zhou, Y., Gogliotti, R.D., Jadhav, S., Zamorano, R., et al. (2011). Discovery, synthesis, and structure-activity relationship development of a series of N-4-(2,5-dioxypyridin-1-yl)phenylpicolinamides (VU400195, ML182): characterization of a novel positive allosteric modulator of the metabotropic glutamate receptor 4 (mGlu(4)) with oral efficacy in an antiparkinsonian animal model. *J. Med. Chem.* 54, 7639–7647. <https://doi.org/10.1021/JM200956Q>.
  38. Garcia-Barrantes, P.M., Cho, H.P., Blobaum, A.L., Niswender, C.M., Conn, P.J., and Lindsley, C.W. (2015). Lead optimization of the VU0486321 series of mGlu1 PAMs. Part 1: SAR of modifications to the central aryl core. *Bioorg. Med. Chem. Lett.* 25, 5107–5110. <https://doi.org/10.1016/j.bmcl.2015.10.013>.
  39. Gutzeit, V.A., Acosta-Ruiz, A., Munguba, H., Häfner, S., Landra-Willm, A., Mathes, B., Mony, J., Yarotski, D., Börjesson, K., Liston, C., et al. (2021). A fine-tuned azobenzene for enhanced photopharmacology in vivo. *Cell Chem. Biol.* 28, 1648–1663.e16. <https://doi.org/10.1016/j.chembiol.2021.02.020>.
  40. Rovira, X., Malhaire, F., Scholler, P., Rodrigo, J., Gonzalez-Bulnes, P., Llebaria, A., Pin, J.P., Giraldo, J., and Goudet, C. (2015). Overlapping binding sites drive allosteric agonism and positive cooperativity in type 4 metabotropic glutamate receptors. *Faseb. J.* 29, 116–130. <https://doi.org/10.1096/FJ.14-257287>.
  41. Klarenbeek, J., Goedhart, J., Van Batenburg, A., Groenewald, D., and Jalink, K. (2015). Fourth-Generation Epac-Based FRET Sensors for cAMP Feature Exceptional Brightness, Photostability and Dynamic Range: Characterization of Dedicated Sensors for FLIM, for Ratiometry and with High Affinity. *PLoS One* 10, e0122513. <https://doi.org/10.1371/JOURNAL.PONE.0122513>.
  42. Pérez-Benito, L., Doornbos, M.L.J., Cordomi, A., Peeters, L., Lavreysen, H., Pardo, L., and Tresadern, G. (2017). Molecular Switches of Allosteric Modulation of the Metabotropic Glutamate 2 Receptor. *Structure* 25, 1153–1162.e4. <https://doi.org/10.1016/J.STR.2017.05.021>.
  43. Harpsøe, K., Isberg, V., Tehan, B.G., Weiss, D., Arsova, A., Marshall, F.H., Bräuner-Osborne, H., and Gloriam, D.E. (2015). Selective Negative Allosteric Modulation Of Metabotropic Glutamate Receptors – A Structural Perspective of Ligands and Mutants. *Sci. Rep.* 5, 2015. <https://doi.org/10.1038/srep13869>.
  44. Du, J., Wang, D., Fan, H., Xu, C., Tai, L., Lin, S., Han, S., Tan, Q., Wang, X., Xu, T., et al. (2021). Structures of human mGlu2 and mGlu7 homo- and heterodimers. *Nature* 594, 589–593. <https://doi.org/10.1038/s41586-021-03641-w>.
  45. Wu, H., Wang, C., Gregory, K.J., Han, G.W., Cho, H.P., Xia, Y., Niswender, C.M., Katritch, V., Meiler, J., Cherezov, V., et al. (2014). Structure of a class C GPCR metabotropic glutamate receptor 1 bound to an allosteric modulator. *Science* 344, 58–64. <https://doi.org/10.1126/science.1249489>.
  46. Christopher, J.A., Orgován, Z., Congreve, M., Doré, A.S., Errey, J.C., Marshall, F.H., Mason, J.S., Okrasa, K., Rucktooa, P., Serrano-Vega, M.J., et al. (2019). Structure-Based Optimization Strategies for G Protein-Coupled Receptor (GPCR) Allosteric Modulators: A Case Study from Analyses of New Metabotropic Glutamate Receptor 5 (mGlu 5) X-ray Structures. *J. Med. Chem.* 62, 207–222. <https://doi.org/10.1021/acs.jmedchem.7b01722>.
  47. Nasrallah, C., Cannone, G., Briot, J., Rottier, K., Berizzi, A.E., Huang, C.Y., Quast, R.B., Hoh, F., Banères, J.L., Malhaire, F., et al. (2021). Agonists and allosteric modulators

- promote signaling from different metabotropic glutamate receptor 5 conformations. *Cell Rep.* 36, 109648. <https://doi.org/10.1016/j.celrep.2021.109648>.
48. Lin, S., Han, S., Cai, X., Tan, Q., Zhou, K., Wang, D., Wang, X., Du, J., Yi, C., Chu, X., et al. (2021). Structures of Gi-bound metabotropic glutamate receptors mGlu2 and mGlu4. *Nature* 594, 583–588. <https://doi.org/10.1038/s41586-021-03495-2>.
  49. Llinas del Torrent, C., Pérez-Benito, L., and Tresadern, G. (2019). Computational Drug Design Applied to the Study of Metabotropic Glutamate Receptors. *Molecules* 24, 1–22. <https://doi.org/10.3390/molecules24061098>.
  50. Lans, I., Díaz, O., Dalton, J.A.R., and Giraldo, J. (2020). Exploring the Activation Mechanism of the mGlu5 Transmembrane Domain. *Front. Mol. Biosci.* 7, 513462. <https://doi.org/10.3389/fmolb.2020.00038>.
  51. Huber, R.G., Margreiter, M.A., Fuchs, J.E., Von Grafenstein, S., Tautermann, C.S., Liedl, K.R., and Fox, T. (2014). Heteroaromatic  $\pi$ -stacking energy landscapes. *J. Chem. Inf. Model.* 54, 1371–1379. <https://doi.org/10.1021/ci500183u>.
  52. Bootsma, A.N., Doney, A.C., and Wheeler, S.E. (2019). Predicting the Strength of Stacking Interactions between Heterocycles and Aromatic Amino Acid Side Chains. *J. Am. Chem. Soc.* 141, 11027–11035. <https://doi.org/10.1021/jacs.9b00936>.
  53. Hauwert, N.J., Mocking, T.A.M., Da Costa Pereira, D., Kooistra, A.J., Wijnen, L.M., Vreeker, G.C.M., Verweij, E.W.E., De Boer, A.H., Smit, M.J., de Graaf, C., et al. (2018). Synthesis and characterization of a bi-directional photoswitchable antagonist toolbox for real-time GPCR photopharmacology. *J. Am. Chem. Soc.* 140, 4232–4243. <https://doi.org/10.1021/jacs.7b11422>.
  54. Gómez-Santacana, X., de Munnik, S.M., Vijayachandran, P., Da Costa Pereira, D., Bebelman, J.P.M., de Esch, I.J.P., Vischer, H.F., Wijtmans, M., and Leurs, R. (2018). Photoswitching the Efficacy of a Small-Molecule Ligand for a Peptidergic GPCR: from Antagonism to Agonism. *Angew. Chem. Int. Ed. Engl.* 57, 11608–11612. <https://doi.org/10.1002/anie.201804875>.
  55. Bahamonde, M.I., Taura, J., Paoletta, S., Gakh, A.A., Chakraborty, S., Hernando, J., Fernández-Dueñas, V., Jacobson, K.A., Gorostiza, P., Ciruela, F., et al. (2014). Photomodulation of G protein-coupled adenosine receptors by a novel light-switchable ligand. *Bioconjug. Chem.* 25, 1847–1854. <https://doi.org/10.1021/bc5003373>.
  56. Donthamsetti, P.C., Winter, N., Schönberger, M., Levitz, J., Stanley, C., Javitch, J.A., Isacoff, E.Y., Trauner, D., Schönberger, M., Levitz, J., et al. (2017). Optical Control of Dopamine Receptors Using a Photoswitchable Tethered Inverse Agonist. *J. Am. Chem. Soc.* 139, 18522–18535. <https://doi.org/10.1021/jacs.7b07659>.
  57. Morstein, J., Romano, G., Hetzler, B.E., Plante, A., Haake, C., Levitz, J., and Trauner, D. (2022). Photoswitchable Serotonins for Optical Control of the 5-HT 2A Receptor. *Angew. Chem.* 134, e202117094. <https://doi.org/10.1002/ange.202117094>.
  58. Broichhagen, J., Podewin, T., Meyer-Berg, H., Von Ohlen, Y., Johnston, N.R., Jones, B.J., Bloom, S.R., Rutter, G.A., Hoffmann-Röder, A., Hodson, D.J., and Trauner, D. (2015). Optical Control of Insulin Secretion Using an Incretin Switch. *Angew. Chem. Int. Ed. Engl.* 54, 15565–15569. <https://doi.org/10.1002/anie.201506384>.
  59. López-Cano, M., Font, J., Aso, E., Sahlholm, K., Cabré, G., Giraldo, J., De Koninck, Y., Hernando, J., Llebaria, A., Fernández-Dueñas, V., and Ciruela, F. (2023). Remote local photoactivation of morphine produces analgesia without opioid-related adverse effects. *Br. J. Pharmacol.* 180, 958–974. <https://doi.org/10.1111/BPH.15645>.
  60. Ferraguti, F., and Shigemoto, R. (2006). Metabotropic glutamate receptors. *Cell Tissue Res.* 326, 483–504. <https://doi.org/10.1007/s00441-006-0266-5>.
  61. Quraishi, S., Gayet, J., Morgans, C.W., and Duvoisin, R.M. (2007). Distribution of group-III metabotropic glutamate receptors in the retina. *J. Comp. Neurol.* 501, 931–943. <https://doi.org/10.1002/CNE.21274>.
  62. Guimaraes-Souza, E.M., and Calaza, K.C. (2012). Selective activation of group III metabotropic glutamate receptor subtypes produces different patterns of  $\gamma$ -aminobutyric acid immunoreactivity and glutamate release in the retina. *J. Neurosci. Res.* 90, 2349–2361. <https://doi.org/10.1002/JNR.23123>.
  63. Zhang, Z., Liu, Y., Luan, Y., Zhu, K., Hu, B., Ma, B., Chen, L., Liu, X., Lu, H., Chen, X., et al. (2020). Activation of Type 4 Metabotropic Glutamate Receptor Regulates Proliferation and Neuronal Differentiation in a Cultured Rat Retinal Progenitor Cell Through the Suppression of the cAMP/PDEN/AKT Pathway. *Front. Mol. Neurosci.* 13, 534310. <https://doi.org/10.3389/fnmol.2020.00141>.
  64. Wang, X., Wang, M., Xu, T., Feng, Y., Shao, Q., Han, S., Chu, X., Xu, Y., Lin, S., Zhao, Q., and Wu, B. (2023). Structural insights into dimerization and activation of the mGlu2–mGlu3 and mGlu2–mGlu4 heterodimers. *Cell Res.* 33, 762–774. <https://doi.org/10.1038/s41422-023-00830-2>.
  65. Friesner, R.A., Murphy, R.B., Repasky, M.P., Frye, L.L., Greenwood, J.R., Halgren, T.A., Sanschagrin, P.C., and Mainz, D.T. (2006). Extra Precision Glide: Docking and Scoring Incorporating a Model of Hydrophobic Enclosure for Protein–Ligand Complexes. *J. Med. Chem.* 49, 6177–6196. <https://doi.org/10.1021/jm051256o>.
  66. Gomez, J., Mary, S., Brabet, I., Parmentier, M.L., Restituito, S., Bockaert, J., and Pin, J.P. (1996). Coupling of metabotropic glutamate receptors 2 and 4 to G alpha 15, G alpha 16, and chimeric G alpha q/1 proteins: characterization of new antagonists. *Mol. Pharmacol.* 50, 923–930.
  67. Brabet, I., Parmentier, M.L., De Colle, C., Bockaert, J., Acher, F., and Pin, J.P. (1998). Comparative effect of l-CCG-I, DCG-IV and  $\gamma$ -carboxy-l-glutamate on all cloned metabotropic glutamate receptor subtypes. *Neuropharmacology* 37, 1043–1051. [https://doi.org/10.1016/S0028-3908\(98\)00091-4](https://doi.org/10.1016/S0028-3908(98)00091-4).
  68. Leach, K., Sexton, P.M., and Christopoulos, A. (2007). Allosteric GPCR modulators: taking advantage of permissive receptor pharmacology. *Trends Pharmacol. Sci.* 28, 382–389. <https://doi.org/10.1016/j.tips.2007.06.004>.

## STAR★METHODS

### KEY RESOURCES TABLE

REAGENT or RESOURCE	SOURCE	IDENTIFIER
<b>Chemicals, peptides, and recombinant proteins</b>		
L-AP4	Tocris Bioscience	Cat#0103 CAS 23052-81-5
Optoglutram (1)	In-house library	CAS 1627840-48-5
VU0415374	In-house library	CAS 1266338-03-7
L-Quisqualic acid	Tocris Bioscience	Cat#0188 CAS 52809-07-1
LY379268	Tocris Bioscience	Cat#2453 CAS 191471-52-0
<b>Critical commercial assays</b>		
HTRF IP-One Gq kit	Revity	62IPAPEC
HTRF IP-One Gi kit	Revity	62a.m.9PEC
Flp-In™ T-REx™ Core Kit	ThermoFisher Scientific	Cat#K650001
Lipofectamine 2000	Thermo Fisher Scientific	Cat#11668019
Polyethyleneimine	Polysciences	Cat#23966
<b>Experimental models: Cell lines</b>		
HEK 293 cells	ATCC	Cat# CRL-1573; RRID:CVCL_0045
<b>Recombinant DNA</b>		
pcDNA3.1 plasmids encoding human mGlu receptors with N-terminal FLAG and SNAP-tags	Revity	
pRK5 qΔNzIC (chimeric Gq/Gi)	Gomez et al. 1996 <sup>66</sup>	
pRK5 EAAC1	Babet et al. 1998 <sup>67</sup>	
<b>Software and algorithms</b>		
ChemDraw Professional 20.0	Revity	<a href="https://revitysignals.com/products/research/chemdraw">https://revitysignals.com/products/research/chemdraw</a>
GraphPad Prism 8.1.1	GraphPad	<a href="https://www.graphpad.com/">https://www.graphpad.com/</a>
MassLynx 4.1	Waters	<a href="https://www.waters.com/waters/es_ES/MassLynx-Mass-Spectrometry-Software">https://www.waters.com/waters/es_ES/MassLynx-Mass-Spectrometry-Software</a>
Thermo Xcalibur 2.2	Thermo Scientific	<a href="https://www.thermofisher.com/order/catalog/product/OPTON-30965">https://www.thermofisher.com/order/catalog/product/OPTON-30965</a>
MestReNova 14	Mestrelab Research	<a href="https://mestrelab.com/software/mnova-software/">https://mestrelab.com/software/mnova-software/</a>
Schrödinger Release 2022-2: Maestro	Schrödinger	<a href="https://www.schrodinger.com/platform/products/maestro/">https://www.schrodinger.com/platform/products/maestro/</a>
BIOVIA Discovery Studio v20.1.0	Dassault Systèmes	<a href="https://www.3ds.com/products-services/biovia/products/molecular-modeling-simulation/biovia-discovery-studio/">https://www.3ds.com/products-services/biovia/products/molecular-modeling-simulation/biovia-discovery-studio/</a>
<b>Other</b>		
Isolera One	Biotage	<a href="https://www.biotage.com/isolera-1-flash-chromatography-instrument">https://www.biotage.com/isolera-1-flash-chromatography-instrument</a>
NMR Varian Mercury 400 MHz	Agilent Technologies	
NMR Ascend 400MHz	Brücker	<a href="https://www.bruker.com/en/products-and-solutions/mr/nmr/ascend-nmr-magnets.html">https://www.bruker.com/en/products-and-solutions/mr/nmr/ascend-nmr-magnets.html</a>
NMR AVANCEIIIHD 500 MHz with TCI Cryoprobe	Brücker	<a href="https://www.bruker.com/en/products-and-solutions/mr/nmr/avance-neo-consoles.html">https://www.bruker.com/en/products-and-solutions/mr/nmr/avance-neo-consoles.html</a>

(Continued on next page)



**Continued**

REAGENT or RESOURCE	SOURCE	IDENTIFIER
HPLC:Waters 2795 Alliance	Waters	<a href="https://www.waters.com/nextgen/es/es/products/chromatography/chromatography-systems.html">https://www.waters.com/nextgen/es/es/products/chromatography/chromatography-systems.html</a>
HPLC: Thermo Ultimate 3000SD	Thermo Scientific	<a href="https://www.thermofisher.com/order/catalog/product/IQLAAEGAAVFCZMAIK">https://www.thermofisher.com/order/catalog/product/IQLAAEGAAVFCZMAIK</a>
HRMS: ultrahigh-performance liquid chromatography (UPLC) Aquity	Waters	<a href="https://www.waters.com/nextgen/es/es/products/chromatography/chromatography-systems.html">https://www.waters.com/nextgen/es/es/products/chromatography/chromatography-systems.html</a>
CoolLED pE-4000 light system	CoolLED	<a href="https://www.cooled.com/products/pe-4000/">https://www.cooled.com/products/pe-4000/</a>
LEDA Array Teleopto	Teleopto	<a href="http://www.teleopto.com/teleopto/led-array-system">http://www.teleopto.com/teleopto/led-array-system</a>
HPLC: Thermo Ultimate 3000SD	Thermo Scientific	<a href="https://www.thermofisher.com/order/catalog/product/IQLAAEGAAVFCZMAIK">https://www.thermofisher.com/order/catalog/product/IQLAAEGAAVFCZMAIK</a>
Evolution 350 UV-Vis spectrophotometer	Thermo Scientific	<a href="https://www.thermofisher.com/order/catalog/product/840-310800">https://www.thermofisher.com/order/catalog/product/840-310800</a>
Tecan Spark M20 multimode microplate reader	Tecan	<a href="https://lifesciences.tecan.com/multimode-plate-reader">https://lifesciences.tecan.com/multimode-plate-reader</a>
PHERASAR FS multimode microplate reader	BMG-Labtech	<a href="https://www.bmglabtech.com/en/microplate-reader/">https://www.bmglabtech.com/en/microplate-reader/</a>

**RESOURCE AVAILABILITY****Lead contact**

Further information and requests for resources and reagents should be directed to and will be fulfilled by the lead contact, Xavier Gómez-Santacana ([xavier.gomez@iqac.csic.es](mailto:xavier.gomez@iqac.csic.es)).

**Materials availability**

All the newly generated materials associated with this study are available from the [lead contact](#) with a completed Materials Transfer Agreement.

**Data and code availability**

- All data reported in this article will be shared by the [lead contact](#) on request.
- This paper does not report original code.
- Any additional information required to reanalyze the data reported in this article is available from the [lead contact](#) upon request.

**EXPERIMENTAL MODEL AND STUDY PARTICIPANT DETAILS**

In the current research the female cell line HEK293 were used. Cells are cultured at 37°C in a humidified atmosphere with 5% CO<sub>2</sub>.<sup>2</sup> Further details are described in the [method details](#).

**METHOD DETAILS****Organic synthesis and chemical characterisation**

All the chemicals and solvents were provided from commercial suppliers and used without purification, except the anhydrous solvents, which were treated previously through a system of solvent purification (*PureSolv*), degasified with inert gases and dried over alumina or molecular sieves (DMF). All the reactions described below were monitored by thin-layer chromatography (60F, 0.2 mm, *Macherey-Nagel*) by visualization under 254 and/or 365 nm lamp. The synthesis of optogluram analogs **3a-d** and **4a-b** is detailed in the supporting information.

Flash column chromatography was performed using silica gel 60 (*Panreac*, 40–63 μm mesh) or by means of SNAP KP-Sil 50 μm (*Biotage*) and/or SNAP KP-C18-HS 50 μm (*Biotage*) columns, automated with Isolera One with UV-Vis detection (*Biotage*).

Nuclear magnetic resonance (NMR) spectra were recorded on a 400 MHz Varian Mercury (*Agilent Technologies*), a 400 MHz Brüker Ascend instrument and 500 MHz Brüker AVANCEIIIHD with TCI Cryoprobe. Data were processed using *Mestre Nova V. 8.1* software (*Mestrelab Research*). <sup>1</sup>H and <sup>13</sup>C chemical shifts are reported in parts per million (ppm) against the reference compound using the signal of the residual non-deuterated solvent [Chloroform (CDCl<sub>3</sub>) δ = 7.26, 1.56 ppm (<sup>1</sup>H), δ = 77.16 ppm (<sup>13</sup>C)]. The following abbreviations have been used to designate multiplicities: s, singlet; d, doublet; t, triplet; m, multiplet; br, broad signal; dd, doublet of doublet; dt, doublet of triplet; ddd, doublet of doublet of doublet. Coupling constants (J) are reported in Hertz (Hz).

Purity determination and absorption UV-Vis spectra were determined with High-Performance Liquid Chromatography Thermo Ultimate 3000SD (*Thermo Scientific Dionex*) coupled to a PDA detector and an LTQ XL ESI-ion trap mass spectrometer (*Thermo Scientific*) or with a Waters 2795 Alliance coupled to a DAD detector (*Agilent 1100*) and an ESI Quattro Micro MS detector (*Waters*). Data from mass and

UV-Vis spectra were analyzed using *Xcalibur* 2.2 SP1 software (Thermo) or *MassLynx* 4.1 software (Waters) HPLC columns used were ZORBAX Eclipse Plus C18 (4.6 × 150 mm; 3.5 μm) and ZORBAX Extend-C18 (2.1 × 50 mm, 3.5 μm). HPLC purity was determined using the following binary solvent system as general method: 0.05% formic acid in 5% MeCN and 0.05% formic acid in 95% water for 0.5 min, from 5 to 100% MeCN in 5 min, 100% MeCN for 1.5 min, from 100 to 5% MeCN in 2 min and 5% MeCN for 2 min. The flow rate was 0.5 mL/min, the column temperature was fixed to 35°C, and wavelengths from 210 to 600 nm were registered. Compound purities were calculated as the percentage peak area of the analyzed compound by UV detection at 254 nm. The isomeric ratio of photoswitchable compounds is given considering the % of absorbance at the isosbestic point of the two species.

All high-resolution mass spectra (HRMS) and elemental compositions were performed on a FIA (flux injected analysis) with ultrahigh-performance liquid chromatography (UPLC) *Aquity* (Waters) coupled to LCT Premier Orthogonal Accelerated Time of Flight Mass Spectrometer (TOF) (Waters). The following binary solvent system is used: from 10% MeCN in 20 mM formic acid to 100% MeCN in 5 min. Data from mass spectra was analyzed by electrospray ionization in positive and negative modes using *MassLynx* 4.1 software (Waters). Given calculated masses are calculated with Chemdraw 20.0. Spectra were scanned between 50 and 1500 Da with values every 0.2 s and peaks are reported as m/z.

### Experimental synthetic procedures

**General synthetic procedure A for compounds 7a and 7b.** HCl (37% aq., 3.1–5.2 eq) was added slowly to a stirred solution of 2-chloroaniline **5** (1.0 eq) in MeOH and the resulting mixture was stirred at 0°C–5°C for 5 min. An aqueous solution of sodium nitrite (1.2 eq) was added dropwise to generate the corresponding diazonium salt, keeping the temperature below 5°C. The mixture was left stirring for 20 min at 0°C–5°C. In parallel, a solution of 3-methoxyaniline **6a** or 2-chloro-5-methoxyaniline **6b** (1.2 eq) and sodium acetate (3.1–5.2 eq) in MeOH/H<sub>2</sub>O (2:1) was prepared in a separate reaction flask and stirred in an ice bath. The freshly prepared diazonium salt solution was kept at 0°C–5°C to avoid degradation and was added dropwise onto the solution of the corresponding aniline **6a-b** and sodium acetate, while keeping the temperature of the reaction at 0°C–5°C. The resulting mixture was stirred at 0°C–5°C for 30 min and cold water was subsequently added to induce the precipitation of the product **7a-b**, which was filtered, washed with precooled water and dried. If the precipitation did not occur, the mixture was extracted twice with EtOAc. The joined organic layers were washed with sat. Na<sub>2</sub>CO<sub>3</sub>, sat. NaHCO<sub>3</sub> and sat. NaCl (x2), dried over anhydrous MgSO<sub>4</sub>, filtered and concentrated *in vacuo*. The obtained residue was purified with automated *flash* direct phase chromatography (n-Hexane/Ethyl acetate 3:1).

**General synthetic procedure B for compounds 3a-d and 4a-b.** The corresponding aromatic carboxylic acid **8a-b**, **9** or **10** (1.5–2.0 eq) with the corresponding aminoazobenzenes **7a-b** (1.0 eq), HATU (3.0 eq) were dissolved in DMF. TEA (5–7.0 eq) was added and the mixture was stirred in an inert atmosphere at 40°C–60°C for 16–48 h. The reaction crude was diluted with EtOAc and was washed with sat. Na<sub>2</sub>CO<sub>3</sub>, sat. NaHCO<sub>3</sub> and sat. NaCl (x2), dried over MgSO<sub>4</sub>, filtered and concentrated *in vacuo*. The residue was purified with automated *flash* reverse phase chromatography (from H<sub>2</sub>O/MeCN 95:5 to MeCN 100% + 0.1% HCOOH).

**(E)-4-((2-chlorophenyl)diazonyl)-3-methoxyaniline (7a).** The general synthetic procedure A was used with 2-chloroaniline (**5**) (500 mg, 3.9 mmol) in MeOH (7.5 mL), HCl (37% aq) (1.0 mL, 33 mmol), sodium nitrite (325 mg, 4.7 mmol) in water (1.8 mL). The second solution was prepared with 3-methoxyaniline (**6a**) (579 mg, 4.7 mmol) and sodium acetate (2.7 g, 33 mmol) in MeOH/H<sub>2</sub>O (2:1, 11.5 mL). Pre-cooled water (150 mL) was added slowly to induce the precipitation of the aminoazobenzene **7a** as an orange solid (587 mg, 57% yield). <sup>1</sup>H NMR (400 MHz, CDCl<sub>3</sub>) δ 7.78 (d, *J* = 9.3 Hz, 1H), 7.68–7.61 (m, 1H), 7.53–7.45 (m, 1H), 7.30–7.26 (m, 2H), 6.32–6.27 (m, 2H), 4.15 (br, 2H), 3.98 (s, 3H). <sup>13</sup>C NMR (101 MHz, CDCl<sub>3</sub>) δ 159.8, 152.2, 149.8, 135.7, 133.9, 130.4, 130.0, 127.4, 119.4, 118.3, 107.8, 97.8, 56.3. HPLC-PDA-MS: *trans* isomer RT = 2.35 min, λ<sub>max</sub> = 478 nm, [M + H]<sup>+</sup> = 262.14; purity (254 nm): 91%.

**(E)-2-Chloro-4-((2-chlorophenyl)diazonyl)-5-methoxyaniline (7b).** The general synthetic procedure A was used with 2-chloroaniline (**5**) (300 mg, 2.4 mmol) in MeOH (5 mL), conc. HCl (1.0 mL, 12.2 mmol), sodium nitrite (195 mg, 2.8 mmol) in water (1.0 mL). The second solution was prepared with 2-chloro-5-methoxyaniline (**6b**) (445 mg, 2.8 mmol) and sodium acetate (1.0 g, 12.2 mmol) in MeOH/H<sub>2</sub>O (2:1, 7.5 mL). The aminoazobenzene **7b** was obtained as an orange solid (592 mg, 85% yield). <sup>1</sup>H NMR (400 MHz, CDCl<sub>3</sub>) δ 7.89–7.84 (app. m, 1H), 7.63 (dd, *J* = 6.2, 3.5 Hz, 1H), 7.53–7.46 (m, 1H), 7.32–7.23 (m, 2H), 6.40 (app. s, 1H), 4.56 (br, 2H), 3.97 (s, 3H). <sup>13</sup>C NMR (101 MHz, CDCl<sub>3</sub>) δ 158.4, 149.5, 147.6, 135.3, 134.3, 130.5, 130.5, 127.4, 118.7, 118.2, 112.8, 98.4, 56.6. HPLC-PDA-MS: *trans* isomer RT = 3.10 min, λ<sub>max</sub> = 420 nm, [M + H]<sup>+</sup> = 296.18; purity (254 nm): 99.5%.

**(E)-3-Chloro-N-4-((2-chlorophenyl)diazonyl)-3-methoxyphenylpicolinamide (3a).** The general synthetic procedure B was used with the aminoazobenzene **7a** (30 mg, 0.11 mmol), 3-chloropicolinic acid (**8a**) (27 mg, 0.17 mmol), HATU (131 mg, 0.34 mmol) and anhydrous TEA (80 μL, 0.57 mmol) in DMF (2.0 mL) at 40°C for 16 h to give the azo compound **3a** (10 mg, 22% yield). <sup>1</sup>H NMR (400 MHz, CDCl<sub>3</sub>) δ 10.25 (br, 1H), 8.55 (dd, *J* = 4.5, 1.4 Hz, 1H), 8.14 (d, *J* = 2.1 Hz, 1H), 7.90 (dd, *J* = 8.2, 1.4 Hz, 1H), 7.83 (d, *J* = 8.7 Hz, 1H), 7.71–7.65 (m, 1H), 7.54–7.50 (m, 1H), 7.46 (dd, *J* = 8.2, 4.5 Hz, 1H), 7.36–7.29 (m, 2H), 7.00 (dd, *J* = 8.8, 2.1 Hz, 1H), 4.11 (s, 3H). <sup>13</sup>C NMR (101 MHz,

$\text{CDCl}_3$ )  $\delta$  161.0, 158.8, 149.6, 146.0, 144.9, 142.6, 141.3, 138.9, 134.7, 133.0, 131.1, 130.6, 127.5, 127.3, 118.3, 118.2, 111.8, 103.5, 56.6. HPLC-PDA-MS: *cis* isomer RT = 2.78 min,  $\lambda_{\text{max}}$  = 268, 434 nm,  $[\text{M} + \text{H}]^+$  = 401.22; *trans* isomer RT = 3.21 min,  $\lambda_{\text{max}}$  = 385 nm,  $[\text{M} + \text{H}]^+$  = 401.17; purity (254 nm): 91.6% *trans* isomer (4.6% *cis* isomer). HRMS (m/z):  $[\text{M} + \text{H}]^+$  calcd for  $\text{C}_{19}\text{H}_{15}\text{Cl}_2\text{N}_4\text{O}_2^+$  401.0567, found 401.0565.

**(E)-N-(4-((2-chlorophenyl)diazanyl)-3-methoxyphenyl)-3-fluoropicolinamide (3b).** The general synthetic procedure B was used with the aminoazobenzene **7a** (30.0 mg, 0.11 mmol), 3-fluoropicolinic acid (**8b**) (24 mg, 0.17 mmol), HATU (131 mg, 0.34 mmol) and anhydrous TEA (80  $\mu\text{L}$ , 0.57 mmol) in DMF (2.0 mL) at 40°C for 16 h to give the azo compound **3b** (35 mg, 79% yield).  $^1\text{H}$  NMR (400 MHz,  $\text{CDCl}_3$ )  $\delta$  10.11 (br, 1H), 8.47 (ddd,  $J$  = 4.4, 1.4 Hz, 1H), 8.18 (d,  $J$  = 2.1 Hz, 1H), 7.83 (d,  $J$  = 8.7 Hz, 1H), 7.72–7.66 (m, 1H), 7.65–7.61 (m, 1H), 7.58 (ddd,  $J$  = 8.4, 4.4, 3.7 Hz, 1H), 7.54–7.49 (m, 1H), 7.36–7.29 (m, 2H), 7.00 (dd,  $J$  = 8.8, 2.2 Hz, 1H), 4.10 (s, 3H).  $^{13}\text{C}$  NMR (101 MHz,  $\text{CDCl}_3$ )  $\delta$  161.3, 160.1, 160.0, 158.6, 149.4, 143.8, 143.7, 142.3, 138.8, 136.8, 136.8, 134.6, 130.9, 130.4, 128.8, 128.8, 127.3, 127.0, 126.8, 118.1, 118.1, 111.6, 103.4, 56.4.  $^{19}\text{F}$  NMR (376 MHz,  $\text{CDCl}_3$ )  $\delta$  –118.19 to –118.28 (m). HPLC-PDA-MS: *cis* isomer RT = 2.72 min,  $\lambda_{\text{max}}$  = 302, 434 nm,  $[\text{M} + \text{H}]^+$  = 385.20; *trans* isomer RT = 3.13 min,  $\lambda_{\text{max}}$  = 391 nm,  $[\text{M} + \text{H}]^+$  = 385.07; purity (254 nm): 90% *trans* isomer (5% *cis* isomer). HRMS (m/z):  $[\text{M} + \text{H}]^+$  calcd for  $\text{C}_{19}\text{H}_{15}\text{ClFN}_4\text{O}_2^+$  385.0863, found 385.0873.

**(E)-3-Chloro-N-(2-chloro-4-((2-chlorophenyl)diazanyl)-5-methoxyphenyl)picolinamide (3c).** The general synthetic procedure B was used with the aminoazobenzene **7b** (30 mg, 0.10 mmol), 3-chloropicolinic acid (**8a**) (24 mg, 0.15 mmol), HATU (116 mg, 0.30 mmol) and anhydrous TEA (100  $\mu\text{L}$ , 0.70 mmol) in DMF (2.0 mL) at 60°C for 48 h to give the azo compound **3c** (9.4 mg, 21% yield).  $^1\text{H}$  NMR (400 MHz,  $\text{CDCl}_3$ )  $\delta$  11.00 (br, 1H), 8.69 (s, 1H), 8.62 (dd,  $J$  = 4.5, 1.4 Hz, 1H), 7.97–7.89 (m, 2H), 7.69 (dd,  $J$  = 7.5, 2.2 Hz, 1H), 7.54 (dd,  $J$  = 7.5, 1.9 Hz, 1H), 7.50 (dd,  $J$  = 8.2, 4.5 Hz, 1H), 7.39–7.30 (m, 2H), 4.13 (s, 3H).  $^{13}\text{C}$  NMR (101 MHz,  $\text{CDCl}_3$ )  $\delta$  161.9, 161.2, 157.5, 149.3, 146.4, 141.3, 138.7, 138.2, 135.1, 133.1, 131.6, 130.7, 127.5, 127.2, 118.2, 117.8, 116.1, 104.4, 56.9. HPLC-PDA-MS: *trans* isomer RT = 5.45 min,  $\lambda_{\text{max}}$  = 391 nm,  $[\text{M} + \text{H}]^+$  = 435.18; purity (254 nm): 98.4%. HRMS (m/z):  $[\text{M} + \text{H}]^+$  calcd for  $\text{C}_{19}\text{H}_{14}\text{Cl}_3\text{N}_4\text{O}_2^+$  435.0177, found 435.0178.

**(E)-N-(2-chloro-4-((2-chlorophenyl)diazanyl)-5-methoxyphenyl)-3-fluoropicolinamide (3).** The general synthetic procedure B was used with the aminoazobenzene **7b** (30 mg, 0.10 mmol), 3-fluoropicolinic acid (**8b**) (21 mg, 0.15 mmol), HATU (116 mg, 0.30 mmol) and anhydrous TEA (71  $\mu\text{L}$ , 0.51 mmol) in DMF (2.0 mL) at 60°C for 48 h to give the azo compound **3d** (7.7 mg, 18.1% yield).  $^1\text{H}$  NMR (400 MHz,  $\text{CDCl}_3$ )  $\delta$  10.85 (br, 1H), 8.72 (app. s, 1H), 8.53 (app. dt,  $J$  = 4.3, 1.4 Hz, 1H), 7.92 (app. s, 1H), 7.71–7.66 (m, 2H), 7.65–7.59 (m, 1H), 7.54 (dd,  $J$  = 7.9, 1.5 Hz, 1H), 7.40–7.30 (m, 2H), 4.11 (s, 3H).  $^{13}\text{C}$  NMR (101 MHz,  $\text{CDCl}_3$ )  $\delta$  192.6, 182.9, 157.5, 154.0, 149.3, 144.4, 144.3, 135.2, 133.5, 131.6, 130.7, 129.2, 129.2, 128.6, 127.5, 127.0, 126.9, 121.1, 118.3, 117.9, 116.0, 104.5, 104.2, 56.8. HPLC-PDA-MS: *cis* isomer RT = 3.17 min,  $\lambda_{\text{max}}$  = 299, 433 nm,  $[\text{M} + \text{H}]^+$  = 417.13; *trans* isomer RT = 3.70 min,  $\lambda_{\text{max}}$  = 390 nm,  $[\text{M} + \text{H}]^+$  = 417.16; purity (254 nm): 73.6% *trans* isomer (11.7% *cis* isomer). The sample contains a known impurity corresponding to compound **3c** (12.7% *trans-3c*, 1.6% *cis-3c*). HRMS (m/z):  $[\text{M} + \text{H}]^+$  calcd for  $\text{C}_{19}\text{H}_{14}\text{Cl}_3\text{N}_4\text{O}_2^+$  435.0177, found 435.0178. HRMS (m/z):  $[\text{M} + \text{H}]^+$  calcd for  $\text{C}_{19}\text{H}_{14}\text{Cl}_2\text{FN}_4\text{O}_2^+$  419.0473, found 419.0470.

**(E)-N-(4-((2-chlorophenyl)diazanyl)-3-methoxyphenyl)thiazole-4-carboxamide (trans-4a) [trans-optogluram-2].** The general synthetic procedure B was used with the aminoazobenzene **7a** (30 mg, 0.11 mmol), the thiazole-4-carboxylic acid (**9**) (22 mg, 0.17 mmol), HATU (131 mg, 0.34 mmol) and anhydrous TEA (80  $\mu\text{L}$ , 0.57 mmol) in DMF (2.0 mL) at 40°C for 16 h to give azo compound **4a** (33 mg, 78% yield).  $^1\text{H}$  NMR (400 MHz,  $\text{CDCl}_3$ )  $\delta$  9.46 (br, 1H), 8.84 (d,  $J$  = 2.1 Hz, 1H), 8.31 (d,  $J$  = 2.1 Hz, 1H), 8.03 (d,  $J$  = 2.1 Hz, 1H), 7.84 (d,  $J$  = 8.7 Hz, 1H), 7.71–7.66 (m, 1H), 7.55–7.49 (m, 1H), 7.37–7.28 (m, 2H), 7.04 (dd,  $J$  = 8.8, 2.2 Hz, 1H), 4.10 (s, 3H).  $^1\text{H}$  NMR (500 MHz, DMSO)  $\delta$  10.69 (br, 1H), 9.31 (d,  $J$  = 2.0 Hz, 1H), 8.58 (d,  $J$  = 2.0 Hz, 1H), 8.00 (d,  $J$  = 2.0 Hz, 1H), 7.68 (dd,  $J$  = 7.9, 1.5 Hz, 1H), 7.67 (dd,  $J$  = 9.2, 2.0 Hz, 1H), 7.64 (d,  $J$  = 8.9 Hz, 1H), 7.58 (dd,  $J$  = 7.9, 1.9 Hz, 1H), 7.51 (td,  $J$  = 7.6, 1.9 Hz, 1H), 7.47 (td,  $J$  = 7.5, 1.5 Hz, 1H), 3.98 (s, 3H).  $^{13}\text{C}$  NMR (101 MHz,  $\text{CDCl}_3$ )  $\delta$  159.0, 158.7, 153.1, 150.9, 149.6, 142.6, 139.0, 134.8, 131.2, 130.6, 127.5, 124.6, 118.3, 118.3, 111.8, 103.7, 56.5. HPLC-PDA-MS: *cis* isomer RT = 2.64 min,  $\lambda_{\text{max}}$  = 285, 433 nm,  $[\text{M} + \text{H}]^+$  = 373.03; *trans* isomer RT = 3.06 min,  $\lambda_{\text{max}}$  = 385 nm,  $[\text{M} + \text{H}]^+$  = 373.22; purity (254 nm): 92.7% *trans* isomer (2.9% *cis* isomer). HRMS (m/z):  $[\text{M} + \text{H}]^+$  calcd for  $\text{C}_{17}\text{H}_{14}\text{ClFN}_4\text{O}_2\text{S}^+$  373.0521, found 373.0518.

**(Z)-N-(4-((2-chlorophenyl)diazanyl)-3-methoxyphenyl)thiazole-4-carboxamide (cis-4a) [cis-optogluram-2].** A 2.5 mM solution of *trans-4a* (**9**) (750  $\mu\text{L}$ , 1.9  $\mu\text{mol}$ ) was irradiated for 5 min with light at 385 nm with the cooled system to give a solution enriched with the title compound.  $^1\text{H}$  NMR (500 MHz, DMSO)  $\delta$  9.46 (br, 1H), 8.84 (d,  $J$  = 2.1 Hz, 1H), 8.31 (d,  $J$  = 2.1 Hz, 1H), 8.03 (d,  $J$  = 2.1 Hz, 1H), 7.84 (d,  $J$  = 8.7 Hz, 1H), 7.71–7.66 (m, 1H), 7.55–7.49 (m, 1H), 7.37–7.28 (m, 2H), 7.04 (dd,  $J$  = 8.8, 2.2 Hz, 1H), 4.10 (s, 3H).

**(E)-N-(4-((2-chlorophenyl)diazanyl)-3-methoxyphenyl)-3-methylfuran-2-carboxamide (4b).** The general synthetic procedure B was used with the aminoazobenzene **7a** (30 mg, 0.12 mmol), the 3-methylfuran-2-carboxylic acid (**10**) (29 mg, 0.23 mmol), HATU (131 mg, 0.34 mmol) and anhydrous TEA (80  $\mu\text{L}$ , 0.57 mmol) in DMF (2.0 mL) at 60°C for 16 h to give azo compound **4b** (21 mg, 49% yield).  $^1\text{H}$  NMR (400 MHz, Chloroform-*d*)  $\delta$  8.24 (br, 1H), 8.03 (d,  $J$  = 2.1 Hz, 1H), 7.81 (d,  $J$  = 8.7 Hz, 1H), 7.72–7.64 (m, 1H), 7.56–7.48 (m, 1H), 7.40 (d,  $J$  = 1.7 Hz, 1H), 7.37–7.27 (m, 2H), 6.89 (dd,  $J$  = 8.8, 2.2 Hz, 1H), 6.43 (d,  $J$  = 1.7 Hz, 1H), 4.09 (s, 3H), 2.48 (s, 3H).  $^{13}\text{C}$  NMR (101 MHz,  $\text{CDCl}_3$ )  $\delta$  158.7, 157.5, 149.6, 143.0, 142.8, 141.8, 138.8, 134.7, 131.1, 130.6, 130.0, 127.5, 118.3, 118.2, 116.3, 111.5, 103.5, 56.6, 11.5. HPLC-PDA-MS: *cis* isomer RT = 2.85 min,  $\lambda_{\text{max}}$  = 286, 435 nm,  $[\text{M} + \text{H}]^+$  = 370.11; *trans* isomer RT = 3.25 min,  $\lambda_{\text{max}}$  = 390 nm,  $[\text{M} + \text{H}]^+$  = 370.19; purity (254 nm): 96.6% *trans* isomer (2.2% *cis* isomer). HRMS (m/z):  $[\text{M} + \text{H}]^+$  calcd for  $\text{C}_{19}\text{H}_{17}\text{N}_3\text{O}_3^+$  370.0953, found 370.0955.

## Photochemical characterisation

### Illumination sources

Two different LED illumination systems were used as light sources: Teleopto and CoolLED. The *Teleopto light* system consists of single or dual wavelength LED Array (model LEDA-X and LEDA2-By respectively) connected to a LED Array Driver (model LAD-1). By the mode switch of LAD-1 LED Array Driver is it possible to choose constant or trigger mode, the latter by means a stimulator (STO mkII, version 1.6) which enables time-controlled pulsed stimulation. The light was delivered from the bottom to the solutions since the LED Array perfectly fits for 96 well-plates and each LED element comes just under each well. Teleopto system set at 12 V intensity and in continuous mode corresponds to 0.09 mW/mm<sup>2</sup> for 365 nm, 0.09 mW/mm<sup>2</sup> for 380 nm, 0.19 mW/mm<sup>2</sup> for 405 nm, 0.13 mW/mm<sup>2</sup> for 420 nm, 0.17 mW/mm<sup>2</sup> for 455 nm, 0.14 mm<sup>2</sup> for 470 nm, 0.10 mW/mm<sup>2</sup> for 500 nm, 0.09 mW/mm<sup>2</sup> for 530 nm and 0.14 mW/mm<sup>2</sup> for 550 nm wavelength. The *CoolLED light* system consists of a liquid light guide accessory (pE-1906, CoolLed) connected to a LED light source (pE-4000, CoolLed). For the photochemical characterization of the samples, the liquid light guide accessory was pointed directly toward each sample placed in transparent 96-well plates so that the light was delivered from the top to the solutions and for 3 min in continuous mode. CoolLED set at 50% intensity corresponds to 1.04 mW/mm<sup>2</sup> for 365 nm, 2.60 mW/mm<sup>2</sup> for 385 nm, 2.10 mW/mm<sup>2</sup> for 405 nm, 0.72 mW/mm<sup>2</sup> for 435 nm, 2.17 mW/mm<sup>2</sup> for 460nm, 1.02 mW/mm<sup>2</sup> for 470 nm, 0.95 mW/mm<sup>2</sup> for 490 nm, 0.3 mW/mm<sup>2</sup> for 500 nm, 0.36 mW/mm<sup>2</sup> for 525 nm, and 1.57 mW/mm<sup>2</sup> for 550 nm light. Potencies were measured using a Thorlabs PM100D power energy meter connected with a standard photodiode power sensor (S120VC).

### UV-Vis spectroscopy materials and methods

The absorption spectra of the photoisomerizable compounds were obtained with solutions 25 μM in DMSO (200 μL of compound solution/well) using a Tecan's Spark 20M Multimode Microplate reader. The samples were measured between 800 and 300 nm with an average time of 50 ms at 2 nm fixed intervals to achieve the full absorption spectra. To evaluate the photoisomerization of the samples and obtain the optimal illumination wavelengths to photoisomerize from *trans* to *cis* configuration by UV-Vis, a continuous illumination for a minimum of 3 min was applied with the corresponding light source mentioned above, on the sample solutions placed in black clear-bottom (Greiner Bio-one) or transparent (Greiner CELLSTAR) 96-well plates (200 μL of compound solution/well). Immediately after the illumination, the samples were read as indicated above with Tecan's Spark 20M Multimode Microplate reader. The effect of repeated light cycles to a sample of 100 μM of compound **4a** in DMSO was evaluated in order to assess the stability of the photoisomerization. Thus, multiple *trans/cis* isomerization cycles were registered by measuring absorbance at a 380 nm wavelength every 2 s with an Evolution 350 UV-Vis spectrophotometer (Thermo Scientific) in the dark and under continuous illumination altering 385 nm and 460 nm wavelengths every 30 s.

### Thermal cis-to-trans relaxation

The thermal relaxation of the *cis*-isomers of optogluram (**1**) and optogluram-2 (**4a**) were the were determined by the kinetic monitoring of the absorbance at 380 nm of 50 μM samples in a mixture of HEPES buffer and DMSO with different proportions: 50%, 10% and 5% DMSO in a quartz cuvette (105-200-85-40, Hellma) with an Evolution 350 UV-Vis spectrophotometer (Thermo Scientific). The samples were pre-illuminated with 385-nm light from the top of the cuvette with the *CoolLED* light source to obtain a high proportion of *cis*-isomer prior to the absorbance reading. The traces obtained were plotted to a one-phase exponential association curve with Graphpad Prism 8.

$$Y = Y_0 + (Y_{plateau} - Y_0) \cdot (1 - e^{-K \cdot t})$$

$$t_{1/2} = \frac{\ln 2}{K} \quad (\text{Equation 1})$$

### Photoisomerization analysis by LC-PDA-MS

The *cis/trans* isomer ratio from photoisomerization of optogluram (**1**) and optogluram-2 (**4a**) was determined by liquid chromatography coupled to a photodiode array and a mass spectrometer detector (LC-PDA-MS). Through the analysis of LC-PDA-MS spectra we quantified the amount of *trans* and *cis* isomers in the dark and upon illumination once reached the photostationary state. The separated peaks were integrated using the PDA channel at the wavelength of the isosbestic point which was previously determined by UV-Vis spectroscopy for each pair of isomers. Illuminations were performed with *CoolLED* light source in microcentrifuge tube containing 150 μL of 1 mM DMSO solution of each compound for 3 min. Then, 10 μL of the stock solution were taken each time and diluted with 90 μL of MeCN in Amber Glass 9 mm Screw Neck Vial to obtain the final 100 μM sample to be analyzed by LC-PDA-MS.

## Pharmacological characterisation

### Materials for pharmacological characterisation

HEK 293 cells were obtained from ATCC CRL-1573 (Molsheim, France). mGlu cDNA constructs were provided by Revvity and the chimeric Gq/Gi and EAAC1 cDNA constructs were previously reported.<sup>66,67</sup> Dulbecco's modified Eagle medium (DMEM), glutamate-free DMEM GlutaMAX, enzyme-free cell dissociation buffer and fetal bovine serum were purchased from Merck-Aldrich. Antibiotics and Polyethylenimine (PEI) were purchased from Merck-Aldrich. The IP<sub>1</sub> assay and cAMP assay kits were provided from REVVITY (Codolet, France).

### Cell culture and transient transfections for pharmacological characterisation

The HEK293 (ATCC, CRL-1573) cells were cultured in Dulbecco's modified Eagle's medium (Gibco DMEM; Thermo Fisher Scientific) supplemented with 10% fetal bovine serum (FBS, Merck-Aldrich) and maintained at 37°C in a humidified atmosphere with 5% CO<sub>2</sub>. Then the cells were transfected with human mGlu receptor by electroporation or lipofectamine transfection following the manufacturer's protocol (*Invitrogen Lipofectamine 2000, Thermo Fisher Scientific*). For those mGlu receptors that are not naturally linked to the phospholipase C (PLC) signaling pathway (mGlu<sub>4,6,8</sub>), a chimeric G<sub>q/i</sub>-protein (G<sub>q</sub> top) was transfected in order to couple receptor activation to the PLC pathway and obtain IP production. We also co-transfected the Excitatory Amino Acid Transporter 3 (EAAC1) to remove the glutamate from the extracellular space, and therefore keep its levels low. The mGlu receptor constructs contained a Flag and SNAP tag to enable the measurement of cell surface receptor expression. Once transfected as previously described<sup>26,30</sup> the cells were seeded in black clear-bottom 96-well plates (*Greiner Bio-one*) at a concentration of 1x10<sup>5</sup> cells/well. At least 2 h before the experiment, the medium was changed to preheated DMEM Glutamax (*Gibco, Thermo Fisher Scientific*), which does not include L-glutamine but contains Glutamax supplement.

### Generation of HEK293 stable rat mGlu<sub>4</sub> inducible cell line

The stably expressing, inducible rat (r)mGlu<sub>4</sub> HEK293 cell line was generated with the Flp-In-T-Rex system according to manufacturer recommendations (*Invitrogen*). The cDNA encoding the rmGlu<sub>4</sub> also contained a Flag and SNAP tag in the N terminus (for detection) and the construct was inserted into the pcDNA5-FRT-TO-GFP plasmid (*Addgene*), where it replaced the GFP. This construct was co-transfected with the recombinase plasmid pOG44 (*Invitrogen*), by electroporation, to allow for targeted integration of the expression vector into the same locus of the Flp-In-T-Rex HEK 293 cells (*Invitrogen*), thereby ensuring homogeneous levels of gene expression. Cells were grown for 48 h, before selection was initiated via the addition of 15 µg/mL blasticidin and 100 µg/mL of hygromycin B. Following induction with 1 µg/mL doxycycline (*Sigma-Aldrich*), inducible expression of the rmGlu<sub>4</sub> receptor on cells was confirmed by an anti-Flag ELISA assay.

### TR-FRET inositol phosphate (IP) accumulation assay

The IP-One HTRF Gq kit assay (REVVITY) was used for the direct quantitative measurement of myo-inositol 1-phosphate in HEK293 cells transiently transfected with the human or rat mGlu receptors according to the transfection methodology described above. Cells were stimulated to induce IP accumulation with various concentrations of orthosteric and/or allosteric compounds, depending on the type of the assay, in HTRF stimulation buffer (REVVITY) for 30 min, at 37°C and 5% CO<sub>2</sub> in both dark and under illumination conditions. For the experiments with illumination to induce photoswitching, the *Teleopto light system* was used. Thus, black transparent-bottom 96-well plates (*Greiner Bio-one*) containing the cultured cells were placed over a single or dual wavelength LED Array (model LEDA-X and LEDA2-By respectively) connected to a LED Array Driver (model LAD-1). The light was delivered from the bottom to the solutions since the LED Array perfectly fits for 96 well-plates and each LED element comes just under each well. Light pulses of 50/50 ms (pulse width/interval) were chosen over continuous illumination to reduce cell overheating (especially for wavelengths with higher energy such as 380 nm) and avoid a loss of robustness of the assay. To avoid effects derived from the fast relaxation of photoisomerizable compounds in aqueous solution after the 30-min stimulation and possible interference with the fluorescence reading, the solutions of every well were removed and fresh stimulation buffer was added prior to the lysis step of the assay protocol. IP1 d2 Reagent solution in HTRF and IP1 Tb Cryptate Antibody solution in lysis buffer were added to each well and the plate was incubated a minimum 1 h at room temperature. TR-FRET fluorescence readings were obtained with PHERAstar FS multimode microplate reader (*BMG-Labtech*) with a delay time of 150 µs between donor excitation and fluorescence readings, as HTRF ratio (665/620). To determine allosteric inactivation, we measured the response of the receptors to high agonist concentrations in both the presence and absence of a competitive antagonist (values used for normalization). Low, high and saturating concentrations of agonists were the same as reported previously.<sup>27</sup>

### TR-FRET cyclic adenosine monophosphate (cAMP) accumulation assay

The cAMP HTRF Gi kit assay (REVVITY) was used for the direct quantitative measurement of cyclic adenosine monophosphate (cAMP) in HEK293 cells stably expressing the rmGlu<sub>4</sub> receptor according to the expression induction protocol described above. Cells in a black transparent-bottom 96-well plates (*Greiner Bio-one*) were stimulated to induce cAMP accumulation with various concentrations of orthosteric and/or allosteric compounds in HTRF stimulation buffer (serum-free DMEM Glutamax supplemented with IBMX 500 µM) for 30 min at 37°C and 5% CO<sub>2</sub> in both dark and light conditions with the addition of Forskolin 0.75 µM in the cells for the last 15 min of incubation. For the experiments with illumination to induce photoswitching, the *Teleopto light system* was used. Thus, black transparent-bottom 96-well plates (*Greiner Bio-one*) containing the cultured cells were placed over a single or dual wavelength LED Array (model LEDA-X and LEDA2-By respectively) connected to a LED Array Driver (model LAD-1). The light was delivered from the bottom to the solutions since the LED Array perfectly fits for 96 well-plates and each LED element comes just under each well. Light pulses of 50/50 ms (pulse width/interval) was chosen over continuous illumination to reduce cell overheating (especially for wavelengths with higher energy such as 380 nm) and avoid a loss of robustness of the assay. To avoid effects derived from the fast relaxation of photoisomerizable compounds in aqueous solution after the 30-min stimulation and possible interference with the fluorescence reading, the solutions of every well were removed and fresh stimulation buffer was added prior to the lysis step of the assay protocol. cAMP Eu-cryptate reagent solution and cAMP-d2 Antibody solution in lysis buffer were added to each well and the plate was incubated a minimum 1 h at room temperature and TR-FRET fluorescence readings were obtained with

PHERAstar FS multimode microplate reader (BMG-Labtech) with a delay time of 150  $\mu$ s between donor excitation and fluorescence readings, as HTRF ratio (665/620).

### Allosteric interactions

For functional interaction studies between the orthosteric agonist, L-AP<sub>4</sub>, and allosteric modulators in the cAMP assay, the following operational model of allosterism was applied.<sup>68</sup>

$$Y = Basal + \frac{(E_M - Basal) \times (([A](K_B + \alpha\beta[B])) + \tau_B[B] \times EC_{50})^n}{(([A](K_B + \alpha\beta[B])) + \tau_B[B] \times EC_{50})^n + (EC_{50}^n \times (K_B[B])^n)} \quad (\text{Equation 2})$$

where Basal is the response in the absence of ligand,  $E_M$  is the maximum response of the system,  $EC_{50}$  is the midpoint of the concentration-response curve of the agonist, [A] and [B] represent the concentrations of the orthosteric agonist, L-AP<sub>4</sub>, and the indicated allosteric ligand, respectively, and  $n$  represents the slope of the transducer function that links receptor occupancy to response.  $K_B$  is the equilibrium dissociation constant of the allosteric ligand,  $K_B$  denotes the capacity of the allosteric ligand to exhibit agonism, and  $\alpha\beta$  represents the combined affinity/efficacy cooperativity parameter describing the effect of the allosteric modulator on agonist function. The derived cooperativity estimates that are greater than 1 indicate positive cooperativity, while values less than 1 but greater than 0 indicate negative cooperativity and values equal to unity denote neutral cooperativity.

### Cell culture and transfection for real time pharmacological assays

HEK293-H188-M1 (HEK293 cells stably expressing the Epac-S<sup>H188</sup> cAMP biosensor) were maintained at 37°C, 5% CO<sub>2</sub> in Dulbecco's modified Eagle medium (DMEM, GIBCO, cat #41965039) supplied with 10% heat-inactivated fetal bovine serum (FBS; GIBCO, cat #11550356).<sup>#1</sup> Cells were grown in T-75 flasks or 10-cm dishes, split when reaching 85–90% confluence and detached by trypsin–ethylenediaminetetraacetic acid (EDTA; Sigma-Aldrich, cat #T3924) digestion. The day before transfection, around  $6.0 \times 10^6$  HEK298-H188-M1 cells were seeded in a 10-cm dish. The following day, the 10-cm dish, with a confluency between 65 and 75%, was taken and the old medium was removed by aspiration, right after 6 mL of DMEM were added. The transfecting agent employed was polyethyleneimine 1 mg/mL solution (PEI; Polysciences, cat#23966) and the PEI/DNA complexes were prepared as follows: Two sterile 1.5 mL tubes were filled with 500  $\mu$ L PBS (GIBCO, cat #11550356) each. Then, 10  $\mu$ g plasmid DNA were added (hmGlu<sub>4</sub>/EAAC1 2:1) to one of them and to the other tube 30  $\mu$ L PEI solution were added. At this point, both tubes were vortexed at full speed (3000 rpm) for 1 min and let stand afterward at room temperature for 10 min. After that, the DNA solution was transferred to the PEI solution, the resulting solution was mixed gently by pipetting up and down three times and it was incubated at room temperature for 3 min. When the time was up, the 1 mL PEI/DNA complexes solution was added dropwise to the 10-cm dish and left in the incubator for 4–5 h (37°C and 5% CO<sub>2</sub>). When the time passed, the old medium containing PEI/DNA complexes was removed and 10 mL of fresh DMEM were added and left in the incubator (37°C and 5% CO<sub>2</sub>) overnight.

### General methods pharmacological reversible photoswitching assays

The assays were carried out using transiently transfected HEK293-H188-M1 cells transiently expressing hmGlu<sub>4</sub> receptor and the excitatory amino acid transporter 1, EAAC1. All assays were performed at room temperature and 48 h after the transfection. The day after the transfection, cells were detached by rinsing once with PBS, followed by incubation with trypsin–EDTA for 5 min until detachment of cells was observed. The detached cells were resuspended with DMEM and 10  $\mu$ L of the resulting suspension were counted using Neubauer Chamber while the cells were being centrifuged at 1300 rpm for 3 min. The supernatant was carefully removed, and cells were resuspended in DMEM complete medium to obtain a cell solution with  $1.0 \times 10^6$  cells/mL. The cell solution was used to seed 125 000 cells per well in a poly-ornithine coated (Poly-L-ornithine hydrobromide, cat#P3655) transparent 96-well microplate (Thermo Scientific Nunc Microwell, cat#10212811) and left at 37°C with 5% CO<sub>2</sub> for approximately 24h. The cAMP EPAC sensor buffer (14 mM NaCl, 50 mM KCl, 10 mM MgCl<sub>2</sub>, 10 mM CaCl<sub>2</sub>, 1 mM N-(2-hydroxyethyl)piperazine-*N'*-ethanesulfonic acid (HEPES), 1.82 mg/mL glucose, pH 7.2) was used as the assay medium in FRET-based experiments. Fluorescence values were measured using a Tecan Spark M20 multimode microplate reader equipped with the Fluorescence Top Standard Module with defined wavelength settings (excitation filter 430/20 nm and emission filters 485/20 and 535/25 nm). The FRET ratio was calculated as the ratio of the donor emission (td<sup>sp173v</sup>, 485 nm) to the acceptor emission (mTurq2 $\Delta$ , 535 nm). The FRET ratio was normalized to the effect of the buffer containing the EC<sub>20</sub> of the agonist (0%) and the response obtained with VU0415374 at the working concentration (100%). External light was applied using the 96-well LED array plate (LEDA Teleopto). Each set of experiments was performed four times with each concentration in triplicate.

### Pharmacological reversible photoswitching assays

48 h after the transfection, the medium from the 96-well microplate was removed by inversion and then 100  $\mu$ L per well of glutamate-free DMEM GlutaMAX (GIBCO, cat#31966021) were added 2 h before starting the assay. Afterward, the DMEM GlutaMAX was removed by inversion and then 80  $\mu$ L per well of the cAMP EPAC sensor buffer containing 100  $\mu$ M of 3-Isobutyl-1-methylxanthine (IBMX; Sigma-Aldrich, cat#15879) were added and it was left at room temperature for 10 min. Meanwhile, a 10x pre-plate containing the final constant concentration of 10  $\mu$ M VU0415374 and optogluram-2, 3  $\mu$ M of VU0415374 and optogluram was prepared using the cAMP EPAC buffer containing IBMX with a EC<sub>20</sub> of L-AP<sub>4</sub> (30 nM). Then, 10  $\mu$ L per well of the cAMP EPAC sensor buffer containing forskolin (final concentration 1  $\mu$ M) was added

and left at room temperature for 15 min. Finally, the compounds and IBMX buffer containing EC<sub>20</sub> of L-AP4 were added and incubated for 1 h at room temperature. After this time, the fluorescence was measured. Then, the plate was continuously illuminated with light at 380 nm for 10 min and fluorescence values were recorded. Immediately after, the plate was illuminated in continuous mode for 10 min with light at 455 nm and fluorescence was measured.

### Computational methods

#### *Preparation of cryoEM structure mGlu<sub>4</sub> receptor (PDB: 7E9H) and docking*

The software used was Schrödinger Release 2022-2: Maestro, Schrödinger, LLC, New York, NY, 2022. The prepared chain R from the cryoEM structure PDB: 7E9H was employed. The rotameric state of amino acid F801 was manually modified toward the membrane. The known binder used for protein refinement was **VU0415374** together with Glide docking with extra precision (Glide-XP). The grid used for the Glide docking was prepared via Receptor Grid Generation protocol followed by the selection of the following amino acids: C636, M663, Y667, L756, L757, W798, S825, S829, S833. The binding pocket was refined by means of Induced-Fit Docking (IFD) using **VU0415374** and the aforementioned amino acids to confine the binding pocket. IFD protocol consisted on an initial Glide Docking (the receptor and ligand van der Waals scaling set to 0.50, and the maximum number of poses to 20) followed by a refinement of residues within 5 Å of ligand poses by Prime and finally a Glide redocking with extra precision. The resulting model from best pose (by both Glide Scoring and visual inspection) was taken as model for the docking of the analogs which was achieved by ligand docking using Glide-XP.

#### *mGlu<sub>6</sub> and mGlu<sub>8</sub> homology modeling based on mGlu<sub>4</sub> cryoEM structure and docking*

The software used was Schrödinger Release 2022-2: Maestro, Schrödinger, LLC, New York, NY, 2022. The cryoEM structure 7E9H was obtained from Protein DataBank. The protomer "Chain R" was selected and then the G protein was extracted. Then the prepared chain R and the sequence mGlu<sub>6</sub> and mGlu<sub>8</sub> (extracted from <https://www.uniprot.org/>, UniProt: O15303 and O00222) were used as input for the homology modeling tool in Maestro. The parameters were left by default and the generated model was subjected to the Protein Reliability script and, afterward, to the Protein Preparation Workflow module. All the ligands used were previously duly prepared using LigPrep (Force field OPLS4, retaining specific chirality). The rotameric state of amino acids F799 in mGlu<sub>6</sub> and F797 in mGlu<sub>8</sub> were manually modified toward the membrane. The grid used for the Glide docking was prepared via Receptor Grid Generation protocol followed by the selection of the following amino acids: I631, T661, Y665, C754, L755, F799, S823, S827, S831 in mGlu<sub>6</sub> and I629, M659, Y663, C752, L753, F797, S821, S825, S829 in mGlu<sub>8</sub>. The binding pocket was refined by means of Induced-Fit Docking (IFD) using **VU0415374** and the aforementioned amino acids to confine the binding pocket. IFD protocol consisted on an initial Glide Docking (the receptor and ligand van der Waals scaling set to 0.50, and the maximum number of poses to 20) followed by a refinement of residues within 5 Å of ligand poses by Prime and finally a Glide redocking with extra precision. The resulting model from best pose (by both Glide Scoring and visual inspection) was taken as model for the docking of the analogs which was achieved by ligand docking using Glide-XP.

### QUANTIFICATION AND STATISTICAL ANALYSIS

All experiments were analyzed using GraphPad Prism 8.1.1 (GraphPad Software, San Diego, CA). All data values are shown as means ± SEM of n independent experiments. The HTRF ratios were transformed to the IP or cAMP concentration produced by the cell with a standard IP or cAMP curve. Then, we normalized the top and the bottom values between 0 and 100% of receptor activation with respect to a control compound pharmacologically well-characterised. The fluorescence obtained in the real time photoswitching assays was normalised by the 0 and 100% of receptor activation with respect to the control **VU0415374**. Potency values (pEC<sub>50</sub>) obtained by concentration-dose were analyzed with two-way ANOVA including the Dunnett correction for multiple testing comparing each compounds potency across receptor subtypes/assays. Activity data obtained in selectivity assays were analyzed with two-way ANOVA including the Dunnett correction for multiple testing comparing activity of in mGlu<sub>4</sub> with the rest of mGlu subtypes. The activity means at every mGlu subtype were compared with an hypothetical activity 0.0 with t-tests. Data from reversible photoswitching assays were analyzed by two-way ANOVA with time as repeated measure and including the Tukey correction for multiple testing, \**p* < 0.05. The comparison between pEC<sub>50</sub>-values in dark conditions or under 380-nm illuminations was performed with unpaired t-tests. The statistical details of experiments can be found in figure and table legends both from the main text and [supplemental information](#).